NeuroImage 100 (2014) 564–579

Contents lists available at ScienceDirect

NeuroImage

journal homepage: www.elsevier.com/locate/ynimg

Determinants of motion response anisotropies in human early visual cortex: The role of configuration and eccentricity

Ryan T. Maloney [a,b,c,*], Tamara L. Watson [d], Colin W.G. Clifford [a,b,c]

[a] School of Psychology, UNSW Australia, Sydney, New South Wales, Australia, 2052
[b] School of Psychology, The University of Sydney, Sydney, New South Wales, Australia 2006
[c] Australian Research Council Centre of Excellence in Vision Science, The University of Sydney, Sydney, New South Wales, Australia 2006
[d] School of Social Sciences and Psychology, The University of Western Sydney, Bankstown, New South Wales, Australia 2200

ARTICLE INFO

Article history:
Accepted 24 June 2014
Available online 1 July 2014

Keywords:
Motion perception
Direction selectivity
fMRI
Optic flow
Radial bias

ABSTRACT

Anisotropies in the cortical representation of various stimulus parameters can reveal the fundamental mechanisms by which sensory properties are analysed and coded by the brain. One example is the preference for motion radial to the point of fixation (i.e. centripetal or centrifugal) exhibited in mammalian visual cortex. In two experiments, this study used functional magnetic resonance imaging (fMRI) to explore the determinants of these radial biases for motion in functionally-defined areas of human early visual cortex, and in particular their dependence upon eccentricity which has been indicated in recent reports. In one experiment, the cortical response to wide-field random dot kinematograms forming 16 different complex motion patterns (including centrifugal, centripetal, rotational and spiral motion) was measured. The response was analysed according to preferred eccentricity within four different eccentricity ranges. Response anisotropies were characterised by enhanced activity for centripetal or centrifugal patterns that changed systematically with eccentricity in visual areas V1–V3 and hV4 (but not V3A/B or V5/MT+). Responses evolved from a preference for centrifugal over centripetal patterns close to the fovea, to a preference for centripetal over centrifugal at the most peripheral region stimulated, in agreement with previous work. These effects were strongest in V2 and V3. In a second experiment, the stimuli were restricted to within narrow annuli either close to the fovea (0.75–1.88°) or further in the periphery (4.82–6.28°), in a way that preserved the local motion information available in the first experiment. In this configuration a preference for radial motion (centripetal or centrifugal) persisted but the dependence upon eccentricity disappeared. Again this was clearest in V2 and V3. A novel interpretation of the dependence upon eccentricity of motion anisotropies in early visual cortex is offered that takes into account the spatiotemporal "predictability" of the moving pattern. Such stimulus predictability, and its relationship to models of predictive coding, has found considerable support in recent years in accounting for a number of other perceptual and neural phenomena.

Introduction

Functional magnetic resonance imaging (fMRI) has recently been proven a useful technique for uncovering broad anisotropies in the tuning properties of visual cortex (in humans and other mammals) to the spatial and spatiotemporal structure of images. These anisotropies have been identified as early as primary visual cortex (V1) for a range of systematically-varied stimulus attributes presented across the visual field, including orientation (Freeman et al., 2011; Furmanski and Engel, 2000; Mannion et al., 2010a; McDonald et al., 2012; Sasaki et al., 2006; Swisher et al., 2010), complex polar form (Mannion and Clifford, 2011; Mannion et al., 2010b) and direction of motion (Beckett et al., 2012; Clifford et al., 2009; Giaschi et al., 2007; Maloney et al., 2013; Raemaekers et al., 2009; Schellekens et al., 2013; Wang et al., 2013). Such anisotropies provide a functional signature of the processing of these attributes across entire populations in visual cortex and have the potential to reveal the strategies used by the visual system to achieve an efficient processing of its inputs.

The focus of the present report is on directional anisotropies, and in particular radial motion biases, in the processing of visual motion in early retinotopic cortex. Pure radial motion is described as either centrifugal (expanding outwards) or centripetal (contracting inwards), and, when centred at the fovea, it describes a trajectory that runs through a range of eccentricities at a single visual field polar angle. Evidence from various sources suggests that the visual system is highly sensitive to this type of motion. Extracellular recordings in non-human primates have indicated radial motion preferences in the middle temporal area MT/V5 (Albright, 1989), V4A (Pigarev et al., 2002), the

* Corresponding author at: School of Psychology, UNSW Australia, Sydney, New South Wales, Australia, 2052. Fax: +61 29385 3641.
E-mail address: r.maloney@unsw.edu.au (R.T. Maloney).

http://dx.doi.org/10.1016/j.neuroimage.2014.06.057
1053-8119/

frontal eye fields (Xiao et al., 2006) and posterior parietal cortex (Steinmetz et al., 1987). There is also an over-representation of neurons tuned to centrifugal motion over other complex motion patterns in the dorsal aspect of the medial superior temporal (MSTd) cortex (Duffy and Wurtz, 1991a, 1991b; Graziano et al., 1994; Lagae et al., 1994; Orban et al., 1992; Tanaka and Saito, 1989; Tanaka et al., 1989). In humans, psychophysical biases for radial motion have been reported (Beardsley and Vaina, 2005; Burr et al., 2001; Morrone et al., 1999), although of the radial motions mixed accounts suggest sensitivity is greater for either centripetal (Edwards and Badcock, 1993; Edwards and Ibbotson, 2007; Giaschi et al., 2007; Raymond, 1994) or centrifugal motion (Ball and Sekuler, 1980; Beardsley and Vaina, 2005; Meese and Anderson, 2002). Further, fMRI studies have shown greater activation for radial over tangential motions in human cortical areas V1–V3 (Beckett et al., 2012; Clifford et al., 2009; Raemaekers et al., 2009; Schellekens et al., 2013; Wang et al., 2013), while fMRI and magnetoencephalography (MEG) studies have indicated that activity in the V5/MT+ complex (the putative human homologue of macaque areas V5/MT and MST; Tootell et al., 1995; Zeki et al., 1991) is enhanced for radial compared to uniformly translating motion (Giaschi et al., 2007; Holliday and Meese, 2005, 2008; Koyama et al., 2005; Morrone et al., 2000; Wall and Smith, 2008; Wall et al., 2008). Functionally, these radial motion biases likely serve important roles in computations related to ego-motion and navigation, such as heading perception and time-to-contact estimation (for reviews see Britten, 2008; Lappe, 2000; Vaina, 1998).

The work of Raemaekers et al. (2009) documented systematic patterns of bias in the response of human early visual cortex to direction of motion. They presented wide-field patterns of coherently-translating random dots that changed their direction of motion a full 360° across a cycle of 100 images, and found that in areas V1, V2 and V3 (but not V5/MT+) the amplitude of the fMRI blood-oxygenation level-dependent (BOLD) response was enhanced for motion radial to the point of fixation (i.e. parallel to the visual field polar angle) compared to tangential (rotational) motion (see also Clifford et al., 2009). A key observation made by Raemaekers and colleagues was that these anisotropies were not uniform across eccentricity. At low eccentricities the strongest responses in areas V1–V3 were elicited by centrifugal motion. At higher eccentricities, however, the responses to centripetal motion tended to be stronger (see also Schellekens et al., 2013; Wang et al., 2013). Raemaekers et al. (2009) note that this dependency on eccentricity may have influenced motion response anisotropies as measured in previous psychophysical and/or fMRI studies, either because the effect was summed or cancelled across eccentricity or because of the particular location in the visual field where the responses were measured. They do not however explore in detail the possible reasons for this change in the anisotropies as a function of eccentricity.

Here, using two different spatial (and temporal) stimulus configurations in two experiments, anisotropies in the response to complex patterns of motion were measured using fMRI in functionally-defined human visual cortical areas V1, V2, V3, V3A/B, hV4 and V5/MT+. Complex motions are parameterised in polar coordinates by the flow angle (relative to a zero degree, radial baseline) typically centred at the point of fixation, whereby motions are characterised as centrifugal, centripetal, rotational or spiral (Clifford et al., 1999; Graziano et al., 1994; Meese and Anderson, 2002; Morrone et al., 1999). The use of complex patterns of motion thus provides a direct manipulation of global motion direction relative to the fovea. In contrast, the uniform translational motion stimuli used previously (e.g. Giaschi et al., 2007; Raemaekers et al., 2009; Schellekens et al., 2013; Wang et al., 2013) provide indirect evidence for radial biases, because they require reference to precise retinotopic cortical maps in order to effect a transformation into polar co-ordinates.

In the first stimulus configuration, wide-field complex motion patterns that systematically changed in flow angle (centred at the fovea) were presented. Anisotropies in the BOLD response to these patterns were apparent, marked by a bias towards the radial motions that depended strongly on eccentricity (particularly in V2 and V3), as with Raemaekers et al. (2009). At the lowest eccentricities, the strongest response was to centrifugal motion patterns and the weakest to centripetal patterns. As eccentricity increased, this pattern gradually shifted to almost the exact opposite pattern: the strongest response was to centripetal motion while the response was weakest to centrifugal motion.

This shift in response bias for motion as a function of eccentricity could be due to the "predictability" of the moving spatial pattern with respect to position in the visual field; such motion predictability is known to have a powerful influence on both perception (Roach et al., 2011; Schwiedrzik et al., 2007; Zhang et al., 2013) and activity in visual cortex (Alink et al., 2010; Kok et al., 2013). In a second experiment, the stimuli were restricted to narrow annuli either close to the fovea or further in the periphery, an arrangement that was intended to reduce the predictability of the moving spatial pattern whilst keeping the local motion information within those annuli the same as it was under the first set of wide-field stimuli. The results were consistent with a radial motion bias in areas V2 and V3 that depended neither on eccentricity nor on whether the motion was centripetal or centrifugal. The results from the two experiments demonstrate a characteristic processing anisotropy in early visual cortex (particularly V2 and V3) for complex motion. This was marked most prominently by radial biases where, for wide-field stimuli but not narrow annuli, the type of radial motion preference (centrifugal or centripetal) depended upon eccentricity. A novel interpretation of these results is provided that emphasises recent developments in theories of predictive coding (e.g. Alink et al., 2010; Enns and Lleras, 2008; Roach et al., 2011; Spratling, 2010; Summerfield and Egner, 2009; Yuille and Kersten, 2006) and how these interactions likely reflect the differential importance of radial motion in the control of ego-motion.

Methods

Subjects

A total of 8 subjects took part in two experiments (ages 24–46 years, 3 female) including the three authors and five who were naive to the theoretical motivations of the study. There were six subjects per experiment, four of whom were common to both. All were experienced in visual psychophysics and fMRI experiments, with corrected-to-normal visual acuity. The experimental protocol came with the approval of the University of Sydney Human Research Ethics Committee.

Stimuli

Visual stimuli consisted of random dot kinematograms (RDKs) presented at 100% coherence and generated with the PsychToolbox 3.0.9 (Brainard, 1997; Pelli, 1997) for MATLAB (7.10 R2010a; The MathWorks, Natick, MA). The RDKs were pre-generated and saved as AVI files, and ranged in flow angle in 16 steps of 22.5°, relative to the radial angle (0°). Thus a flow angle of 0° produced centrifugal motion, ±180° gave centripetal motion, 90° counter-clockwise motion and −90° clockwise motion (see Fig. 1C). Flow angles intermediate to these four "cardinal" flows result in spiral motions of varying pitch (Beardsley and Vaina, 2005; Graziano et al., 1994; Meese and Anderson, 2002). All were centred at the fovea and set against the mean background luminance of the display, and, in the wide-field configuration, within an annular region with an inner border at 0.75° and an outer border at 6.28° (Figs. 1A–B). The outer edge of the stimuli was slightly less than the maximum possible on the display apparatus (a radius of 7.15°; see below). Stimuli in the second experimental configuration were identical to those in the wide-field configuration except that the RDKs were presented (in separate runs) within much narrower annuli: an inner annulus of 0.75–1.88° and a more eccentric, outer annulus of 4.82–6.28° (Figs. 1E–F). The positions of these two annuli were the same as the

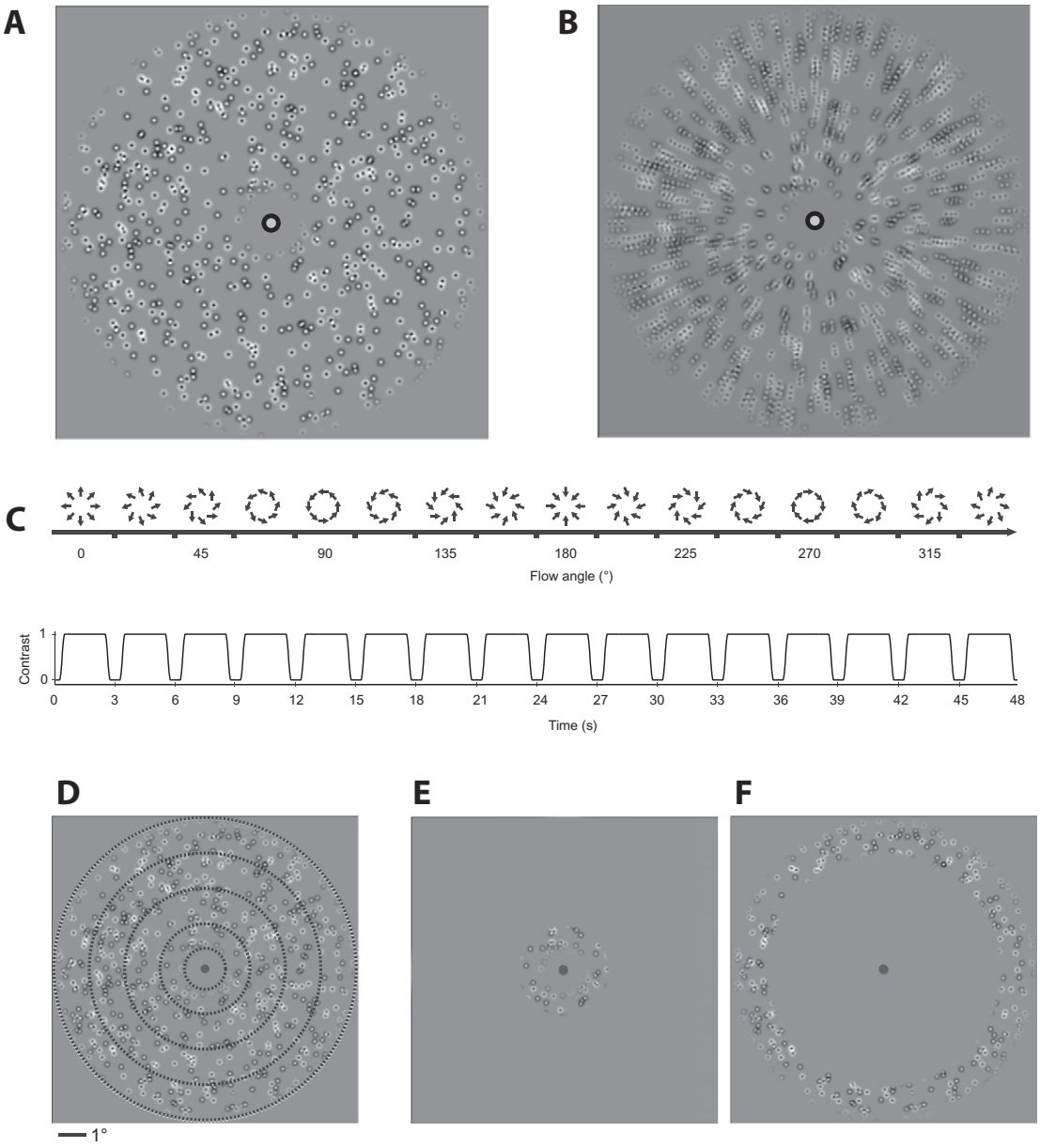

Fig. 1. Stimulus configuration and functional magnetic resonance imaging (fMRI) duty cycle. *A*: A schematic illustration of a single frame from a random dot kinematogram (RDK) in the wide-field configuration showing the Laplacian of Gaussian (LoG) dots. *B*: A stylised "time-lapsed" image showing the sum of 3 frames (each separated by 83 ms) from the RDK shown in *A*, illustrating how the motion of either a centrifugal (0°) or centripetal (180°) flow angle pattern might appear when integrated over time. *C*: The phase-encoded stimulus duty cycle for the wide-field stimulus experiment, showing a single full cycle (48 s). The 16 complex motion flow angles advanced by 22.5° with each volume acquisition (3 s). Each RDK was presented at 100% coherence and at full contrast for 2 s. Contrast was ramped on and off with a temporal raised cosine over 250 ms, while an additional period of 250 ms preceded and succeeded each RDK where only a blank screen of the mean luminance background was displayed. *D*: Another single frame from the wide-field stimulus showing the four eccentricities by which the spatial extent of the stimulus was divided up for analysis. The concentric black dashed lines show the four eccentricities. Note that these black lines are a guide only and did not appear on the actual stimulus. *E*: An example single RDK frame illustrating the spatial extent of the inner annulus (0.75–1.88°) in the narrow annulus condition. *F*: An example single RDK frame showing the spatial extent of the outer annulus (4.82–6.28°) in the narrow annulus condition. Note that the scale bar shown at the bottom left of *D* is also appropriate for *E* and *F*.

innermost and outermost eccentricities analysed following the wide-field stimulus configuration. The aim of restricting the motion stimuli to within these annuli was to reduce the predictability of the moving spatial pattern compared to the larger flow patterns presented in the wide-field stimulus, whilst keeping the local properties of the stimuli constant at those eccentricities. Note that what was visible within the inner and outer annuli had the same characteristics as that displayed within the same space in the wide-field stimulus, in other words, the spatial extent of the RDK patterns was restricted in the second experiment but dot size, density and speed did not change from the wide-field stimulus. Dot contrast at the annular borders was ramped with a raised cosine spatial profile of 0.09°. Each RDK was presented at full contrast for 2 seconds (see Design and Procedure below).

The RDKs, which were similar to the ones described in Maloney et al. (2013), were made up of 100% peak contrast dots with spatially

band-pass isotropic Laplacian of Gaussian (LoG) profiles (Dakin and Mareschal, 2000):

$$\nabla^2 G(x,y,\sigma) = \frac{1}{\sigma^2}\left(1-\frac{x^2+y^2}{\sigma^2}\right)\exp\left(-\frac{\left(x^2+y^2\right)}{2\sigma^2}\right), \quad (1)$$

with $\sigma = 0.05°$ (examples given in Fig. 1). Micro-patterns had a peak spatial frequency of 10.6 cycles/°. The spatially band-pass profile of the LoG dots served to minimise temporal integration along dot trajectories resulting in artefactual oriented blur known as "motion streaks" (Apthorp et al., 2011; Geisler, 1999) which have the potential to confound radial biases for motion with radial biases for orientation (Clifford et al., 2009). In the first frame of each RDK, the contrast of each dot was randomly assigned to be either a full contrast increment or decrement from the background luminance, with equal probability of each polarity. The mean speed of the RDKs was 1.78°/s. While this speed may seem somewhat slow (and, based on the data from the macaque, possibly suboptimal for motion-selective areas such as V5/MT+; Lagae et al., 1994; Tanaka and Saito, 1989), it was chosen to further limit the influence of motion streaks (Geisler, 1999).

The complex motion patterns of the RDKs were generated according to the algorithm outlined in Clifford et al. (1999), where the position of each dot on a given frame of the display was sampled in a discrete manner from a continuous trajectory according to its distance from the focus of radial motion (i.e. the fixation point). Dot speed was thus scaled by the distance from fixation. A constant dot density was maintained across the duration of each RDK according to the "wraparound" procedure described in Clifford et al. (1999). Dots were positioned randomly in the first frame of an RDK, with a uniform density per unit area of the stimulus aperture. In a centrifugal motion pattern (with a flow angle of 0°), some dots would escape the outer boundary of the aperture with the frames that followed. When these dots were "wrapped around", they were randomly repositioned back into the stimulus aperture, but under the constraint that dot density was maintained (Clifford et al., 1999). The local transients accompanying dot disappearance and reappearance within the aperture were thus greatest for the purely centripetal and centrifugal motions, while dots in the purely rotational motions (±90°) never escape the borders of the aperture. To ensure that the number of local transients was uniform across the full set of complex motions tested, the "effective coherence", or the correspondence between a dot's position from one frame to the next, was set to the same value (99.3%) across all flow angles (Maloney et al., 2013).

Apparatus and magnetic resonance imaging

Stimuli were projected through the Faraday shield on a back-projection screen positioned behind the scanner bore with the use of a Dell 5100MP digital projector (Dell, Round Rock, TX) with resolution 1024 × 768 pixels, a vertical refresh of 60 Hz and a mean luminance of 275 Cd/m^2. Subjects viewed the stimuli through a rear-facing mirror positioned on the scanner head coil at a total viewing distance of 167 cm, giving a display viewing angle of 19° × 14.3°. Stimulus presentation was synchronised to the scanner trigger pulse and driven by a PC with an nVidia Quadro FX 1700 M graphics adapter. The subjects' behavioural responses were captured with the use of a LU400-PAIR Lumina response pad (Cedrus, San Pedro, CA). Across the two experiments, reliable eye position data was obtained for five subjects using the MR-compatible EyeLink1000 infrared eye tracking system (SR Research, Mississauga, ON, Canada), with the use of the EyeLink Toolbox (Cornelissen et al., 2002) for MATLAB.

Functional MRI was performed with a Philips Achieva 3 T TX scanner (Philips Healthcare, Best, The Netherlands) with a whole-head SENSE coil. Subject head position was stabilised with comfortable foam padding to minimise head movement artefacts ("NoMoCo" system; Cambridge Research Systems, Rochester, Kent). Functional volumes were obtained using a boustrophedon, field-echo (T_2*-weighted) echo-planar imaging (EPI) sequence with the following parameters: time to echo (TE): 32 ms, volume time to repetition (TR) = 3000 ms, flip angle = 90°, field of view = 192 × 69 × 192 mm, matrix = 128 × 128, and with an isotropic voxel size of 1.5 × 1.5 × 1.5 mm. The images were acquired in 46 interleaved, ascending slices in a tilted coronal plane covering the occipital lobes as well as portions of the posterior parietal and inferior temporal cortices. The tilt of the slices was positioned to be approximately perpendicular to the orientation of the calcarine sulcus. To aid in coregistration of functional images and regions of interest (ROIs; see below) a T_1-weighted whole-head anatomical volume (voxel size = 1 × 1 × 1 mm) was also obtained for each subject within each scanning session using a turbo field-echo protocol for enhanced grey/white matter contrast. Data analysis was performed with the Statistical Parametric Mapping package for MATLAB (SPM8; Friston et al., 2007) and custom MATLAB routines.

Design and procedure

In the wide-field stimulus experiment a continuous presentation (phase-encoded) paradigm was used in the display of stimuli (Freeman et al., 2011; Maloney et al., 2013; Mannion et al., 2010a, 2010b; Raemaekers et al., 2009). Engel (2012) provides a recent exposition of the advantages of phase-encoded designs when using fMRI to study the cortical representation of continuously-defined stimulus parameters. The stimulus duty cycle is illustrated in Fig. 1C. The sixteen complex motion patterns were presented in a systematic, stepwise manner, where the flow angle advanced 22.5° with each 3000 ms functional volume acquisition. A full stimulus cycle ran for 48 s and 7.25 cycles were completed within a single run. To avoid abrupt transitions between RDKs, there was a 250 ms blank period at the beginning and end of each volume, while the contrast of the RDKs was also ramped on and off with a temporal raised cosine profile over further periods of 250 ms. As such, stimuli were presented at full contrast for 2000 ms and were each separated in time by a 500 ms blank period (see Fig. 1C). The flow angles were advanced in a clockwise (i.e. decreasing from 337.5°) or counter-clockwise direction (i.e. increasing from 0°) on alternating runs, of which subjects completed at least 6.

The narrow annuli experiment took the form of a block design. The focus of this experiment was to explore the differences between the pure radial motions at different eccentricities, and between the radial and rotational motions, so only the 4 cardinal flow angles were presented in separate blocks. Subjects completed at least 6 counterbalanced runs each of the inner annulus and outer annulus conditions (Figs. 1E–F). The duration of a single block was 12 s, during which RDKs at one of the four cardinal flow angles was presented within either the inner or outer annulus. Each stimulus block was separated by a fixation block of the same length where the screen was blank apart from the fixation spot. Stimulus blocks ran in the order centrifugal (0°), counter-clockwise rotation (90°), centripetal (180°) and finally clockwise rotation (−90°), and this order was cycled through three times within a run. The block order was reversed on alternate runs.

Fixation task

Eye position and spatial attention were controlled for during all functional scans with a challenging task subjects performed at fixation, which involved monitoring a small central fixation point (0.19° diameter) and reporting a subtle shift in its luminance by holding down one of 2 buttons on the response pad. The fixation spot fluctuated between two luminance levels during the run on average every 2000 ms, with a random jitter around this value of ±500 ms. Performance on this task was quantified by the mutual information (MI) between the luminance level (an entropy of 1 bit) and the subject response. Furthermore, reliable eye position data was obtained with the use of the Eyelink1000 system for two subjects in the wide-field experiment and four subjects in the narrow annulus experiment (two of these subjects were common

to both experimental designs). Together, the eye position and fixation task data confirmed that the subjects were fixating consistently upon the fixation spot for the duration of the functional scans. The fixation task data further indicated that subjects' attention was tied to the point of fixation. For the wide-field stimulus, the peak MI of the response had an average latency (an approximation of reaction time) of 385 ms (with range = 331–502 ms). The mean across subjects and runs of the peak MI was 0.62 bits (with range 0.55–0.71 bits). In the second experiment, for the inner annulus condition, the mean peak MI was 0.65 bits (range = 0.58–0.72), while for the outer annulus the mean peak MI was 0.66 bits (range = 0.59–0.74). The average latency of the peak MI was 415 ms (range = 314–550 ms) for the inner annulus condition, and 432 ms (range = 317–625) for the outer annulus condition.

Across the two stimulus configurations/experiments, subjects made very few saccades outside a 1° radius from the fixation point, and the mean interblink interval (IBI) was similar to that measured in normal subjects performing a visual task outside the MRI scanner environment (5.97 s; Johnston et al., 2013). There were no obvious differences in the mean trends in BOLD fMRI observed in the wide-field and narrow annulus stimulus configurations for those subjects where eye tracking data was obtained compared to those where it was not. Across all runs in the wide-field stimulus experiment (each with a total duration of 5 min 57 s), subjects made an average of 6.5 saccades of an amplitude greater than 1° but less than 1.5° from fixation, and an average of 5.25 saccades of an amplitude greater than 1.5°. The mean IBI was 5.34 s. Across all runs for the narrow annulus experiment (where runs had a total duration of 5 min), in the inner annulus condition, an average of 1.94 saccades of an amplitude greater than 1° but less than 1.5° were made, while there was an average of 0.89 saccades of greater than 1.5° amplitude. For the outer annulus condition, on average 3.44 saccades between 1° and 1.5° occurred, while an average of 1.5 saccades of an amplitude greater than 1.5° occurred. The average IBI for the inner annulus condition was 7.08 s, and for the outer annulus condition it was 5.73 s. All saccades with an amplitude greater than 1° from fixation were pooled across all runs in the wide-field stimulus experiment for the two subjects with reliable eye tracking data. Circular correlations (Mardia and Jupp, 2000) indicated that there was no systematic dependence of the number of saccades made on the stimulus motion flow angle ($r = 0.12$, $p = 0.22$). Further, whenever a saccade did occur it tended to be downwards and to the left ($r = 0.28$, $p < 0.001$).

Retinotopic mapping and region of interest (ROI) definition

Visual cortical regions of interest V1, V2, V3, V3A/B, hV4 and V5/MT+ were defined for the analysis of fMRI data for each individual subject in separate scans prior to the two primary experiments. Phase-encoded retinotopic mapping was performed using well-established protocols involving rotating wedge and expanding/contracting ring stimuli to define polar angle and eccentricity maps, respectively (Engel et al., 1994, 1997; Larsson and Heeger, 2006; Wandell and Winawer, 2011; Wandell et al., 2007). The topographically organised maps of angular and eccentricity preferences obtained using this method have been described in detail in previous papers from this laboratory (Goddard et al., 2010; Maloney et al., 2013; Mannion et al., 2010a). Briefly, the wedge and ring stimuli produced a "travelling wave" of activity that allowed for each voxel's preferred polar angle (wedge) and eccentricity (rings) to be determined, based on the temporal phase of the best-fitting sinusoid. The data were projected onto a computationally-flattened representation of both occipital lobes where the visual areas could be manually defined using the Stanford Vision, Imaging Science and Technology Laboratory mrVista software suite for MATLAB (http://white.stanford.edu/software/). Visual areas defined according to this scheme included V1–V3 and hV4 which share a foveal representation at the occipital pole, and areas V3A and V3B (which were not analysed separately) that share a dorsal foveal representation on the border of the dorsal portion of V3. Area hV4 was defined as a hemifield representation of the contralateral visual field on the ventral border of V3, which itself is sometimes labelled VP (Goddard et al., 2011; Pitzalis et al., 2006). An additional separate localiser was also performed to define cortical area V5/MT+, a strongly motion-selective region near the ascending limb of the inferior temporal sulcus (Tootell et al., 1995; Zeki et al., 1991). The design of the localiser has been described previously (Goddard et al., 2010; Maloney et al., 2013; Seymour and Clifford, 2012) and was based on a comparison of the response to coherently-moving versus static random dots presented in separate blocks (with interleaved fixation-only blocks). V5/MT+ was defined as a lateral cluster of voxels showing a greater response to the moving than to the static dots (Dumoulin et al., 2000; Fischer et al., 2012; Huk et al., 2002; Smith et al., 2006) in a general linear model specification of the data using SPM8.

Analysis

Spatial preprocessing of all fMRI data sets (the retinotopic, localiser and experimental scans) was performed in SPM8. Images were corrected for between- and within-run head movement artefacts and aligned to the whole-head structural image acquired within the same session using normalised mutual information-based coregistration. Each ROI was coregistered and resliced to fit the space of the experimental data using fourth-degree B-spline interpolation.

In the wide-field experiment, the mean BOLD signal intensity to the 16 complex motion flow angles was computed for each ROI. The eccentricity phase maps obtained in the retinotopic scans were used to examine the BOLD response within each ROI as a function of eccentricity. Voxels with preferred eccentricities within four different concentric annular regions were examined in each ROI: 0.75–1.88°, 1.88–3.34°, 3.34–4.82° and 4.82–6.28° (see Fig. 1D). Collectively these four eccentricity ranges covered the entire spatial extent of the stimulus and roughly corresponded to the eccentricities analysed by Raemaekers et al. (2009). Table 1 (below) provides the mean number of voxels (across subjects) sampled for each ROI at each eccentricity.

To obtain the mean response, the first quarter-cycle (4 volumes; 12 s) of each run was discarded (in order to allow the BOLD intensity to reach a steady equilibrium after the onset of stimuli) and the response time course was shifted forwards by +2 volumes (6 s) to compensate for the sluggish nature of the haemodynamic response. Data from runs where the motion flow angles advanced in a clockwise direction were temporally reversed and combined with those that advanced counter-clockwise. The data were then high-pass filtered (cut-off period = 128 s) and averaged across the voxels within the ROI for each eccentricity. The BOLD response was then converted into a percentage signal change (PSC) and normalised for each run according to the following:

$$\mathrm{PSC}(T) = 100 \times \left(b(T) - \overline{b}\right)/\overline{b}, \tag{2}$$

where $b(T)$ is the mean BOLD signal intensity across all voxels for each discrete volume, T, in the run (after correction for the haemodynamic

Table 1
Mean number of voxels (across subjects, $n = 6$) in each ROI for each eccentricity analysed in the wide-field stimulus configuration.

Eccentricity range (°)				
	0.75–1.88	1.88–3.34	3.34–4.82	4.82–6.28
ROI	# voxels			
V1	842 (±112)	523 (±66)	757 (±142)	924 (±237)
V2	417 (±99)	451 (±74)	607 (±143)	797 (±216)
V3	352 (±64)	408 (±64)	548 (±179)	724 (±189)
V3A/B	65 (±24)	69 (±18)	197 (±53)	481 (±88)
hV4	299 (±58)	345 (±94)	401 (±144)	277 (±49)
V5/MT+	13 (±5)	23 (±7)	38 (±12)	36 (±16)

Note. Numbers in parentheses give one standard error of the mean.

lag) and $\bar{b}$ is the mean value across all volumes. Normalising the PSC in this way centres the mean value at zero (such that responses across the full range of flow angles have a zero sum). Data were averaged across runs and stimulus cycles to produce a final 16-item vector describing the mean percentage signal change across flow angles for each eccentricity for each ROI. The anisotropies in the response for each eccentricity were assessed using circular correlation (Mardia and Jupp, 2000). To guard against spurious correlations due to Type 1 errors given the temporally low-pass nature of the haemodynamic response, a bootstrap procedure (Efron and Tibshirani, 1993) was used to establish a distribution of circular correlations that would be expected under the null hypothesis. The statistical significance of the r values resulting from the circular correlations of the real data could then be evaluated against this null distribution. This procedure involved first drawing a set of 16 independent random values from the standard normal distribution and convolving them with the canonical haemodynamic response function for a 3000 ms TR, as obtained from SPM8. This was repeated 2000 times to generate a distribution of noisy "surrogate" data sets of the BOLD response to the 16 complex motions. Just as with the actual data, half of these surrogate data sets were then "temporally" reversed and added to the other half. A circular correlation was then performed on each surrogate data set to arrive at a null distribution of 1000 r values. This process was repeated 10 times, and the 95th percentile at each distribution was obtained. If the resulting circular correlation for the actual data exceeded the mean 95th percentile for each of the null distributions, then the result was considered significant ($p < 0.05$). Note that circular correlations are always positive (Mardia and Jupp, 2000) and were performed (for each eccentricity and each ROI) across the 16-item set of values that represented the mean BOLD response to the 16 different complex motion flow angles across the 6 subjects.

The goal of the narrow annulus experiment was to examine the change in response to the four cardinal motion flow angles within and across the inner and outer eccentricities stimulated in the wide-field experiment, when the motion was presented within only those regions. To limit (mask) the analysis to just those voxels within each ROI active during stimulation periods, a general linear model (GLM) contrast of the response to all four motion flow angles compared to fixation only was performed in SPM8, separately for the inner and outer annulus conditions. Those voxels with a significant t statistic ($p < 0.05$, 1-tailed, uncorrected) in the resulting maximum intensity projection maps (t-maps) then served as a mask for each ROI in the analysis that followed. An average BOLD time course across those voxels was computed; giving an $n \times 100$ matrix for each masked ROI, where 100 was the total number of volumes per run and n was the number of runs per eccentricity condition (at least 6). As with the wide-field data, these time courses were high-pass filtered (cut-off period = 128 s) and the PSC calculated using Eq. (2), where the mean across volumes, $\bar{b}$, was calculated with the exclusion of the very first block in the run (a fixation block; 4 volumes, 12 s). Finally, a mean time course for each stimulus type was computed by averaging across the repeat blocks within a run (3 blocks per stimulus), and then by averaging across the runs. Note that the mean time course for each stimulus is given as a 12 s stimulus block (4 volumes) followed by a 12 s fixation block (also four volumes; see Fig. 2A).

The resulting mean time courses were examined using a similar logic to Larsson et al. (2006). The aim was to arrive at a "response

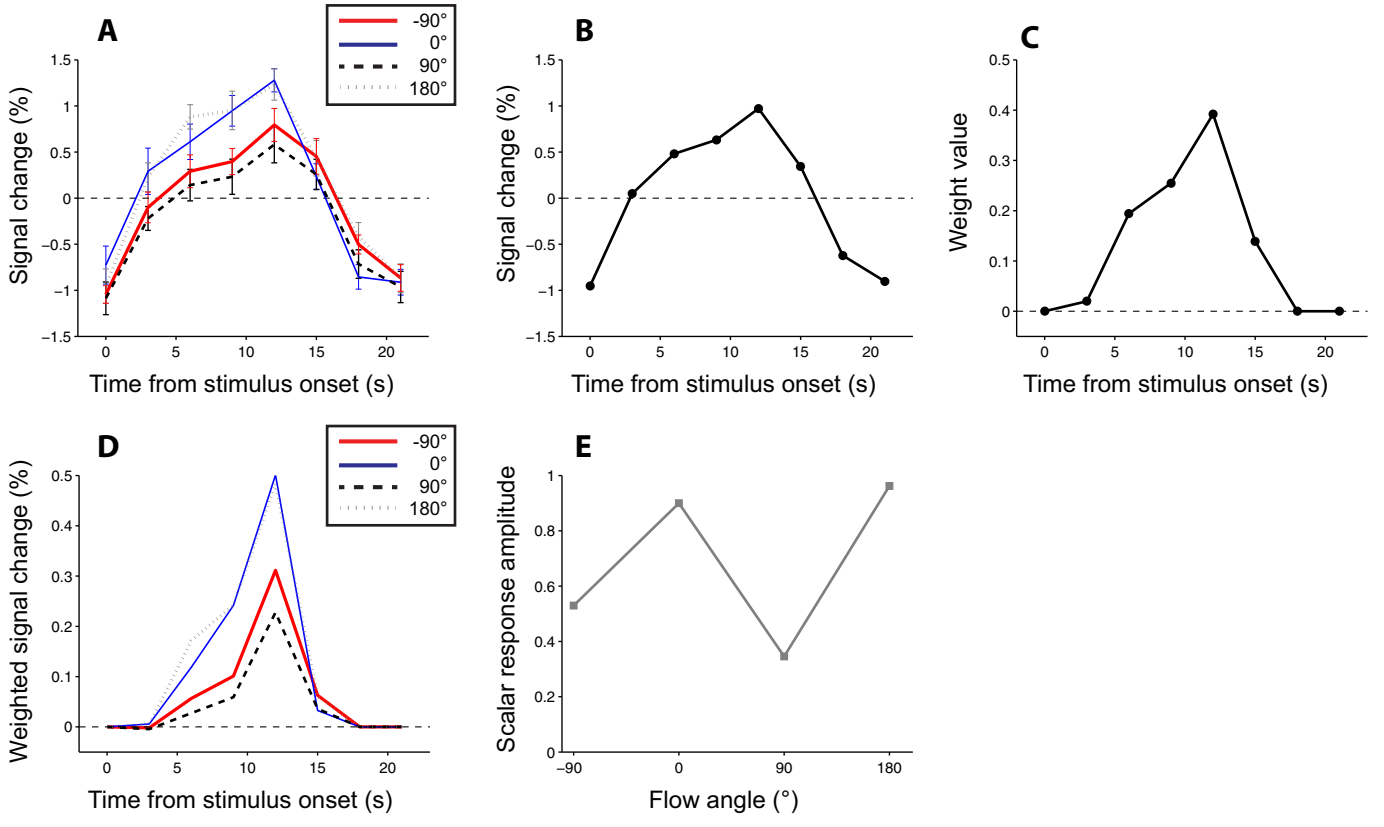

Fig. 2. Demonstration of the procedure used for arriving at scalar response amplitude values for each motion flow angle in the inner or outer narrow annulus conditions. The example data shown come from a single subject during the outer annulus condition, from area V3. *A*: Example original time courses for the four motion flow angles (shown as separate lines). Error bars show standard errors of the mean across repeat stimulus blocks and runs. *B*: The mean time course across all motion flow angles. *C*: Weight values, w_r, obtained for each 3 s time point (volume), obtained by half-wave rectifying the mean time course and then normalising to sum to unity. *D*: Weighted time courses obtained by multiplying each original time course shown in *A* by the weight values shown in *C*. *E*: Scalar response amplitude values for each of the four motion flow angles obtained by summing along each of the four weighted time courses shown in *D*. Scalar response amplitude values such as the examples shown here formed the basis of the analysis for the narrow annulus experiment.

template" for each subject that provided an objective way to select a meaningful time epoch for analysis of the response to the different motion flow angles, whilst accommodating for the slight differences in the temporal profiles of each subject's haemodynamic response. The steps in this approach are depicted in Fig. 2 with an example data set from a single subject in the outer annulus condition, starting with the mean time courses for the four motion flow angles (Fig. 2A). In the analysis, firstly, the average time course across the four motion conditions was calculated for each subject and each annulus condition (Fig. 2B). This average time course was then half-wave rectified so that all values less than zero (i.e. less than the mean) were made equal to zero, thereby serving to remove parts of the response profile that were not stimulus-related. The values for each time point (volume), τ, were then divided by their sum to provide a set of weights, w_τ, where $0 \leq w_\tau < 1$, and $\Sigma w_\tau = 1.0$ (Fig. 2C). The original mean time courses were then multiplied by the weights (Fig. 2D) and summed to provide a scalar response amplitude value for each motion condition (Fig. 2E). Comparisons between motion conditions and eccentricity (inner annulus or outer annulus) for each ROI were then made with two-factor repeated measures analyses of variance (ANOVAs) across the amplitude values for each subject. To confirm that our findings did not depend on the specifics of the analysis, the data from the narrow annulus experiment were also analysed by computing the mean BOLD response time courses for the four motion flow angles indexed relative to the mean response on fixation-only blocks, rather than to the mean response across all (stimulus and fixation) blocks. The mean responses across volumes within each of those motion time courses were then analysed in the same way and produced nearly identical results to the response template approach just described. Note that, in analysing the results of both the wide-field and narrow annulus stimulus configurations, no statistical comparisons were performed across visual areas. Since each visual area was considered to constitute a separate statistical "family" (Ludbrook, 1998), no correction for conducting multiple tests (one for each of the 6 ROIs) was performed (see also Mannion et al., 2010a).

Results

Wide-field stimulus configuration

In the first experiment with the wide-field stimulus configuration subjects were presented with RDKs that cycled through 16 different complex motion flow patterns with their focus centred at the fovea. The mean response to the complex motions was computed within four different ranges of preferred eccentricity for six visual cortical areas. The results for each visual ROI (shown as the average across the 6 subjects) are given in Fig. 3. To aid in describing the pattern of anisotropy in the response to the different motions, the best-fitting cosinusoid (with phase and amplitude free to vary) is also shown for each eccentricity in each ROI. Circular correlations (Mardia and Jupp, 2000) were performed for each eccentricity in each ROI, and where those circular correlations were significant ($p < 0.05$, by bootstrap procedure, see Materials and Methods) the phase of the best fitting cosinusoid is shown as an arrow on the abscissa in Fig. 3. This gives an indication of where the peak response across flow angles occurred for each particular eccentricity. Table 2 gives the results of the circular correlations as well as the best-fitting phase values for data at each eccentricity and each ROI as shown in Fig. 3.

For all visual areas except V5/MT+ and V3A/B there were distinct anisotropies in the response to the different complex motions presented, dominated by clear preferences for centrifugal or centripetal radial motion. This was characterised by a peak response over centrifugal motion (0°) at the inner eccentricity ranges (0.75–1.88° and 1.88–3.34°) and, in almost complete antiphase to the response at the inner eccentricities, a peak over centripetal motion (±180°) for the outermost eccentricity range (4.82–6.28°). The anisotropies at the third eccentricity (3.34–4.82°) tended to be smaller than the other eccentricity ranges, though in V1–V3 there was still a peak close to centrifugal (significant only in V3). The response to rotational motion (±90°) meanwhile was close to the mean across all flow angles (i.e. a PSC of close to 0%). As the arrows in Fig. 3 indicate, these effects were significant at the outermost eccentricity only in V1, all but the third eccentricity in V2, at all eccentricities in V3, and at the second eccentricity only (1.88–3.34°) in hV4. The anisotropies were not significant at any eccentricity in V3A/B or V5/MT+, although the trends observed in V3A/B were qualitatively similar to areas V1–V3 (see Fig. 3 and Table 2). The results are consistent with radial biases for the cortical response to motion as has been demonstrated in earlier fMRI work (Beckett et al., 2012; Clifford et al., 2009; Raemaekers et al., 2009; Schellekens et al., 2013; Wang et al., 2013), although unlike previous work this was demonstrated directly using variations of complex motion patterns centred foveally.

Narrow-annulus stimulus configuration

The second experiment sought to further explore the nature of the motion anisotropies and their interaction with eccentricity as observed in the wide-field stimulus experiment. In a block design, the global "predictability" of the radial motion trajectories was interrupted by presenting the four cardinal complex motion patterns within a narrow annulus of either small (inner annulus: 0.75–1.88°) or large (outer annulus: 4.82–6.28°) eccentricity (as in Figs. 1E–F). For each ROI and for the inner and outer annulus conditions a scalar response amplitude value was obtained for each of the four cardinal motion flow angles, which are given as the separate lines in Fig. 4, presented as averages across subjects. Factorial repeated measures ANOVAs with annulus (inner and outer) and motion flow angle (centrifugal, counter-clockwise, centripetal and clockwise) as factors were performed on these data for each ROI, the outcomes of which are provided in Table 3.

As Table 3 shows, in no ROI was the annulus × flow angle interaction significant (all $p > 0.05$). Main effects for flow angle did reach significance in all ROIs ($p < 0.05$) except for V5/MT+ ($p = 0.08$). The main effect of annulus was significant in V3 only ($p = 0.01$), which reflects the greater overall BOLD response for stimuli presented within the inner annulus over the outer annulus. Notably, the main effect for flow angle was greatest in V2 and V3 which is also where the results with the wide-field stimulus were most compelling.

Because there were no significant annulus × flow angle interactions in any ROI the data were collapsed across annulus and motion type. Single response values for "rotational" motion were produced by averaging the clockwise and counter-clockwise motions across both annulus conditions, as well as single values for centrifugal and centripetal motion. Centrifugal and centripetal were further averaged to produce a single result for "radial" motion at each ROI. Averaged radial and rotational responses are given as the separate bar plots within each panel in Fig. 4. The aim was to assess the strength of any possible radial bias (i.e. overall rotational against overall radial motion) and also probe whether there was any preference for one type of radial motion over the other (i.e. overall centrifugal against overall centripetal). These comparisons were made with paired samples *t*-tests for each ROI, the results of which are given in Table 4.

Radial bias, indexed as a larger overall response to the two radial motions over the two rotational motions was significant in V2 and V3 only ($p = 0.008$ and $p = 0.004$, respectively). This result approached significance in areas V3A/B and hV4 ($p = 0.062$ and $p = 0.065$, respectively) but not in V1 or V5/MT+ ($p > 0.1$). The difference between the overall responses to centrifugal and centripetal was significant only in V1 ($p = 0.04$), reflecting the slightly greater mean response to centrifugal (mean response amplitude = 1.28) over centripetal (mean response amplitude = 1.16). Again, the significant radial bias in V2 and V3 complements the results obtained in the wide-field stimulus experiment.

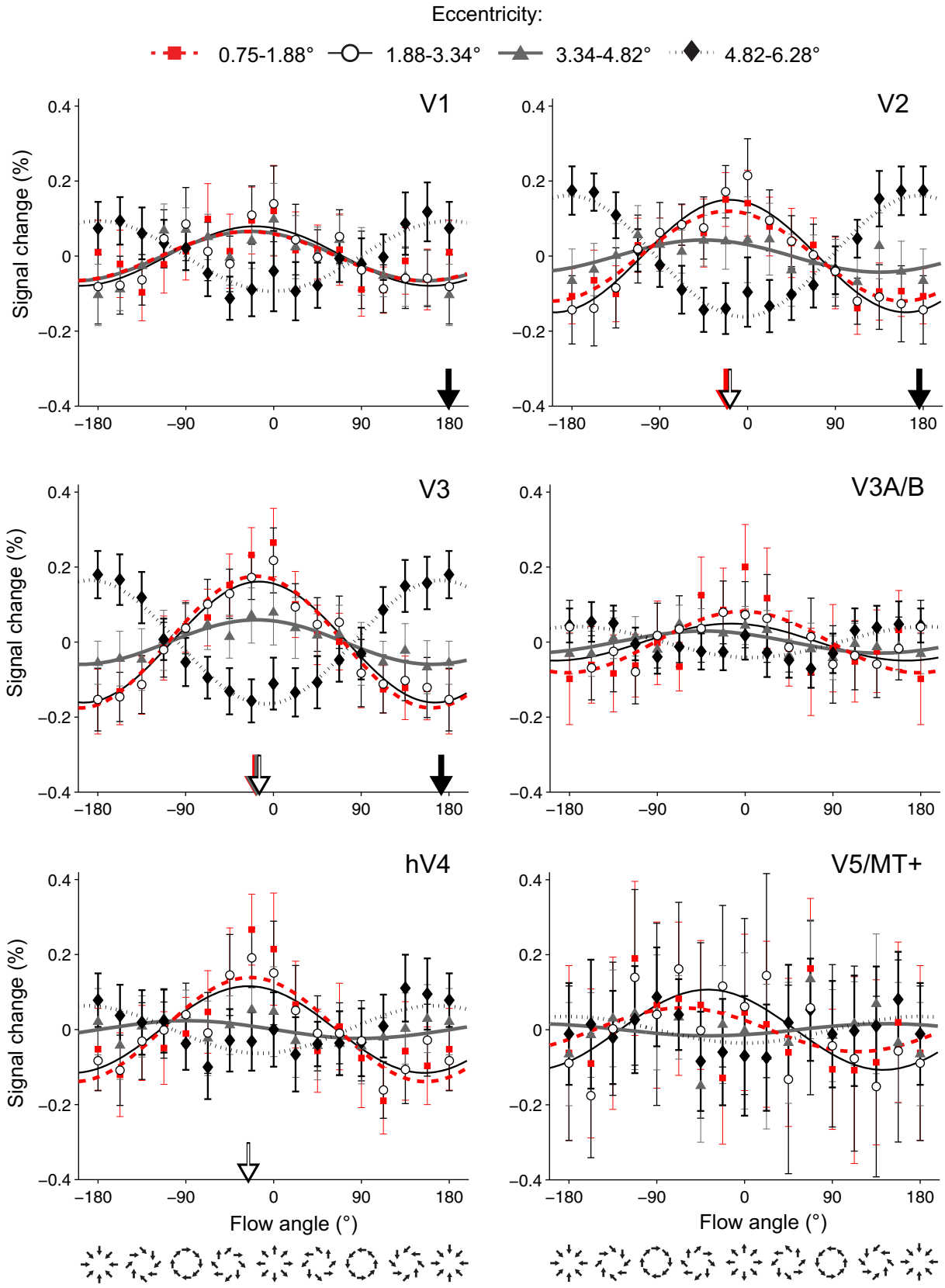

Fig. 3. Results for the wide-field stimulus configuration. Each panel shows the mean BOLD percentage signal change across the six subjects (±1 standard error) at four different eccentricities for each of the six different visual cortical regions of interest. Note that data for centripetal motion is wrapped so that it appears at both +180° and −180° on the abscissa. Symbols show the mean data for the different eccentricities, while smooth lines show the best-fitting cosinusoid. Downward-pointing arrows on the abscissa show the phase of the best-fitting cosinusoid where the circular correlation was significant. The colour of the arrows is the same as the data symbols for the four different eccentricity ranges.

Table 2
Results of circular correlations (r) and phase of the best-fitting cosinusoid for each eccentricity and each ROI for the wide-field stimulus experiment.

	Eccentricity range (°)							
	0.75–1.88		1.88–3.34		3.34–4.82		4.82–6.28	
ROI	r	Phase (°)	r	Phase (°)	r	Phase (°)	r	Phase (°)
V1	0.53	−26	0.64	−19	0.64	−24	0.87**	179
V2	0.90**	−21	0.93***	−18	0.55	−45	0.94***	176
V3	0.90**	−18	0.94***	−14	0.86*	−17	0.96***	172
V3A/B	0.46	−2	0.48	−15	0.51	−42	0.55	−173
hV4	0.69	−24	0.75*	−26	0.25	−89	0.63	167
V5/MT+	0.19	−64	0.51	−38	0.03	145	0.24	−180

*$p < 0.05$; **$p < 0.01$; ***$p < 0.001$ (uncorrected), according to the null distribution of r values obtained via bootstrap procedure.

Table 3
Results of factorial ANOVAs ($n = 6$) of scalar response amplitude data from the narrow annulus experiment.

	Interaction	Main effect: Flow angle	Main effect: Annulus
ROI	$F_{3,15}$	$F_{3,15}$	$F_{1,5}$
V1	0.82	5.03*	1.86
V2	2.84	10.20***	0.14
V3	0.31	10.84***	16.07**
V3A/B	0.25	4.12*	1.73
hV4	0.31	3.72*	1.29
V5/MT+	0.42	2.76	0.01

* $p < 0.05$, ** $p < 0.01$, *** $p < 0.001$.

Test for stimulus edge effects in the wide-field stimulus configuration

It is possible that the observed changes in the motion flow angle response anisotropies with eccentricity in the wide-field stimulus configuration could be due to suppressive interactions at the edges of the stimulus, or shifts in the spatial representation of the stimulus in response to motion direction (Liu et al., 2006; Whitney and Bressler, 2007; Whitney et al., 2003). A second analysis of the data was performed in an attempt to address this possibility. The SPM maximum intensity projection maps (t-maps) obtained in the GLM used to mask the voxels in each ROI in the narrow annulus experiment (i.e. the contrast of all motion flow angles against fixation-only; see Methods) were again used to mask each ROI before computing the mean response, this time with the data from the wide-field stimulus experiment. This was done separately for the inner and outer narrow annuli for the 4 subjects common to both the wide-field and narrow annulus experiments. In this way, only those voxels within each ROI that were active significantly above baseline (fixation) in the narrow annulus experiment were included in the second analysis of the wide-field stimulus data. Masking the voxels in this way should prevent any influence of suppressive interactions at the edge of the stimulus. Furthermore, it also obviates the need to refer to eccentricity maps in selecting the voxels for analysis, since these maps are inevitably going to suffer from some measurement error and there is likely to be some imprecision inherent in binning voxels by eccentricity, particularly in higher areas where population receptive fields (pRFs) are larger, there are fewer voxels, and the visual

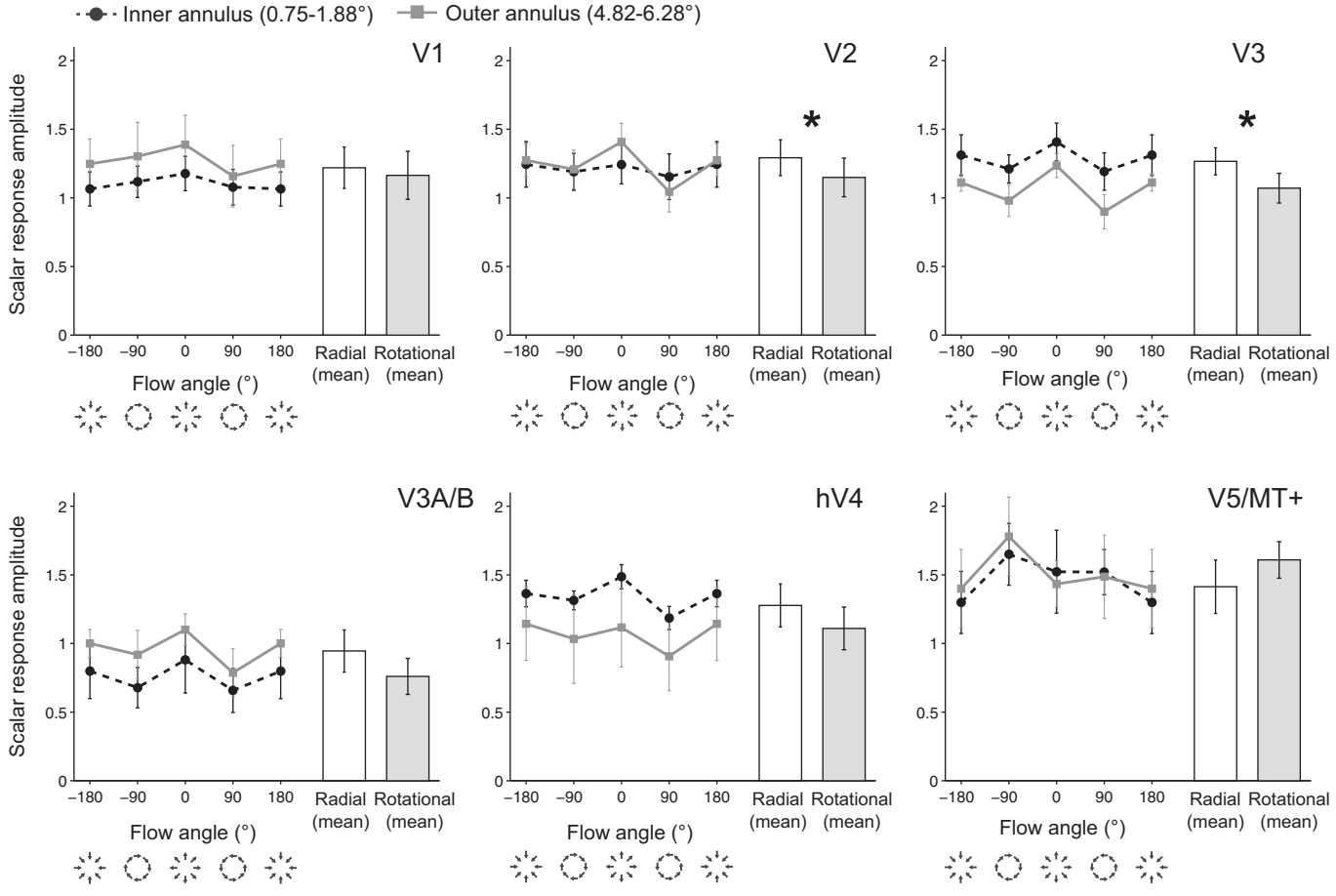

Fig. 4. Mean scalar response amplitude data across subjects (±1 standard error) for the narrow annulus experiment, showing both the inner annulus (black dashed lines) and outer annulus (grey lines) conditions, for each of the six regions of interest. Note that responses for centripetal motion are wrapped so that they appear at both +180° and −180° on the abscissa. The bar plots in each panel show the mean radial motion response (in white; obtained by collapsing across centripetal and centrifugal motion and across annulus) and the mean rotational motion response (in grey; obtained by collapsing across clockwise and counter-clockwise motion and across annulus). Vertical lines on the bars give ±1 standard error. * $p < 0.05$.

Table 4
Results of paired-samples *t*-tests ($n = 6$) comparing scalar response amplitude data for the narrow annuli experiment after collapsing across annulus and/or motion type (radial or rotational).

	Mean centrifugal vs. mean centripetal motion	Mean radial vs. mean rotational motion
ROI	t_5	t_5
V1	2.79*	1.37
V2	2.0	4.24**
V3	2.08	4.96**
V3A/B	1.22	2.39
hV4	0.56	2.35
V5/MT+	0.87	−1.99

*$p < 0.05$, **$p < 0.01$.

field map is less clearly defined (e.g. V3A/B, hV4, V5/MT+; Amano et al., 2009; Dumoulin and Wandell, 2008). As in the original analysis of the wide-field data, circular correlations as well as a cosine fit were applied to each annulus in each ROI, and the statistical significance of the circular correlation was determined by the bootstrapped distribution of *r* values expected under the null hypothesis. The results of this analysis are given in Fig. 5 below, while the phase of the best-fitting cosinusoid and the circular correlation *r* statistics are provided in Table 5. As Fig. 5 and Table 5 indicate, the outcome of this second analysis was very similar (and in some instances stronger) to the original analysis of the wide-field data at the innermost (0.75–1.88°) and outermost (4.82–6.28°) eccentricities. Circular correlations were significant at both inner and outer annuli in areas V1, V2 and V3, but not elsewhere. A simple comparison of the original data in Fig. 3 with those in Fig. 5 reveals qualitatively very similar trends at the respective spatial locations of the stimuli. This additional analysis strongly suggests that the modulation in the motion response anisotropies with eccentricity as observed in the wide-field stimulus configuration is not due to suppressive influences at the edge of the stimulus, or noise associated with limitations in the travelling-wave method used in obtaining the eccentricity maps.

Discussion

This study sought to explore directional anisotropies, and in particular radial biases, in the visual cortical response to motion. Two different configurations of fully-coherent complex motion stimuli, both centred on the fovea, were displayed while subjects fixated centrally. One experiment involved wide-field patterns while in the other they were restricted to a narrow annulus, either close to the fovea or further in the periphery. Anisotropies in the mean response in early visual cortical areas were observed. With the wide-field configuration the form of these anisotropies was modulated by stimulus eccentricity. In early visual areas V1-hV4 the anisotropies were characterised by a preference for radial motion; at small eccentricities (up to 3.34°) there was a tendency towards a greater mean BOLD response to centrifugal motion and a reduced or even suppressed response to centripetal; whereas at the widest eccentricity tested (4.82–6.28°) the form of these anisotropies changed such that there was an enhanced response to centripetal motion and a supressed response to centrifugal. These influences were significant according to a circular correlation at all eccentricities in V3 and some eccentricities in V1, V2 and hV4. V3A/B showed a qualitatively somewhat similar response pattern although it was not significant. There were no clear anisotropies or effects of eccentricity in V5/MT+. In the second experiment these dependencies on eccentricity were explored by presenting the motion within one of two narrow annuli that corresponded to the innermost and outermost eccentricities analysed in the wide-field experiment. Doing so reduced the predictability of the moving spatial pattern but preserved its local characteristics within the stimulated regions of the visual field. With this configuration the eccentricity effects largely disappeared, yet there was still a significantly greater response to radial versus rotational motion overall in areas V2 and V3. Finally, the data from the wide-field experiment were re-analysed but the voxels in each ROI were masked by the SPM *t*-maps of the most active voxels in the narrow annulus configurations. The results of this analysis were very similar to the initial eccentricity analysis, suggesting that the change in the response anisotropies were not a consequence of stimulus edge artefacts.

Given its high density of direction-selective cells, area V5/MT has a long-established role in motion perception, both in non-human primates (Allman and Kaas, 1971; Dubner and Zeki, 1971; Maunsell and Van Essen, 1983) and in humans (Greenlee, 2000; Tootell et al., 1995; Zeki et al., 1991). It is perhaps somewhat surprising then that no clear evidence for radial biases or other motion anisotropies was apparent in V5/MT+. Although the present report is more concerned with motion anisotropies in early retinotopic cortex (e.g. V1–V3), this point is worthy of some discussion. Several reports have shown increased BOLD intensity or enhanced MEG in V5/MT+ in response to radial motion over random or uniformly translating motion (Giaschi et al., 2007; Holliday and Meese, 2005, 2008; Koyama et al., 2005; Morrone et al., 2000; Wall and Smith, 2008; Wall et al., 2008). However, as with the present study, other previous reports have also failed to find evidence for anisotropies in the response to motion direction in V5/MT+ using fMRI (Beckett et al., 2012; Raemaekers et al., 2009; Wang et al., 2013). There are a number of possible factors that may have contributed to this. Of course, the lack of observed motion anisotropies here and previously does not necessarily imply that they do not exist; statistical power may have been insufficient in this experiment or it is possible that fMRI lacks the necessary resolution or sensitivity to detect these particular interactions (Bartels et al., 2008). The eccentricity mapping for V5/MT+ is less precise and there are also generally fewer voxels available than with other visual cortical areas, including those analysed here (Wandell et al., 2007). Human V5/MT+ (and its constituent parts, e.g. MST) possesses different columnar and topographic organisation to earlier retinotopic cortex, and while this region consists of at least two visual field maps (and probably more; Amano et al., 2009; Kolster et al., 2010), they are notoriously difficult to map with fMRI (Huk et al., 2002; Tootell et al., 1995; Wandell and Winawer, 2011; Wandell et al., 2007; Zimmermann et al., 2011). Further, neurons in macaque areas V5/MT and particularly MST have large receptive fields, often requiring stimuli as large as 40–80° to elicit a vigorous increase in spike rate (Albright, 1989; Duffy and Wurtz, 1991a; Lagae et al., 1994; Raiguel et al., 1997; Tanaka and Saito, 1989); while MST cells also tend to prefer higher speed stimuli (Duffy and Wurtz, 1997; Lagae et al., 1994; Tanaka and Saito, 1989). It is possible that the wide-field motion stimulus used here was too small or not of a fast enough speed (an average of 1.78°/s) to drive direction-selective populations in V5/MT+ to the point where modulations with the pattern of complex motion could be measured at the voxel level.

The graded change in the motion response anisotropies with eccentricity was significant only in early visual cortex (V2 and V3). While making comparisons across different cortical regions based on BOLD activity is inherently problematic (Smith et al., 2011), the pRFs in the other cortical ROIs that represent later stages in visual processing (V3A/B, hV4 and V5/MT+) are larger and are likely to include a greater degree of overlap across the different eccentricity ranges tested, especially in V5/MT+ (Amano et al., 2009). The phase-encoded expanding/contracting rings stimulus employed here to compute the eccentricity maps, though widely used, is not without its limitations and there may have been some error associated with separating the maps into the relatively narrow eccentricity ranges tested here. This would be more the case in the higher areas and particularly in V5/MT+, which is perhaps another reason why no motion anisotropies were observed there (cf. Raemaekers et al., 2009; Wang et al., 2013). Extrapolating from the data of Dumoulin and Wandell (2008; Fig. 9), the average pRF centred over the 3rd eccentricity range (i.e. at 4.08° eccentricity) is expected to be 0.55° in diameter in V1, 0.83° in V2, and 1.6° in V3. Thus it is reasonable to assume that the overlap of pRFs in the 3rd

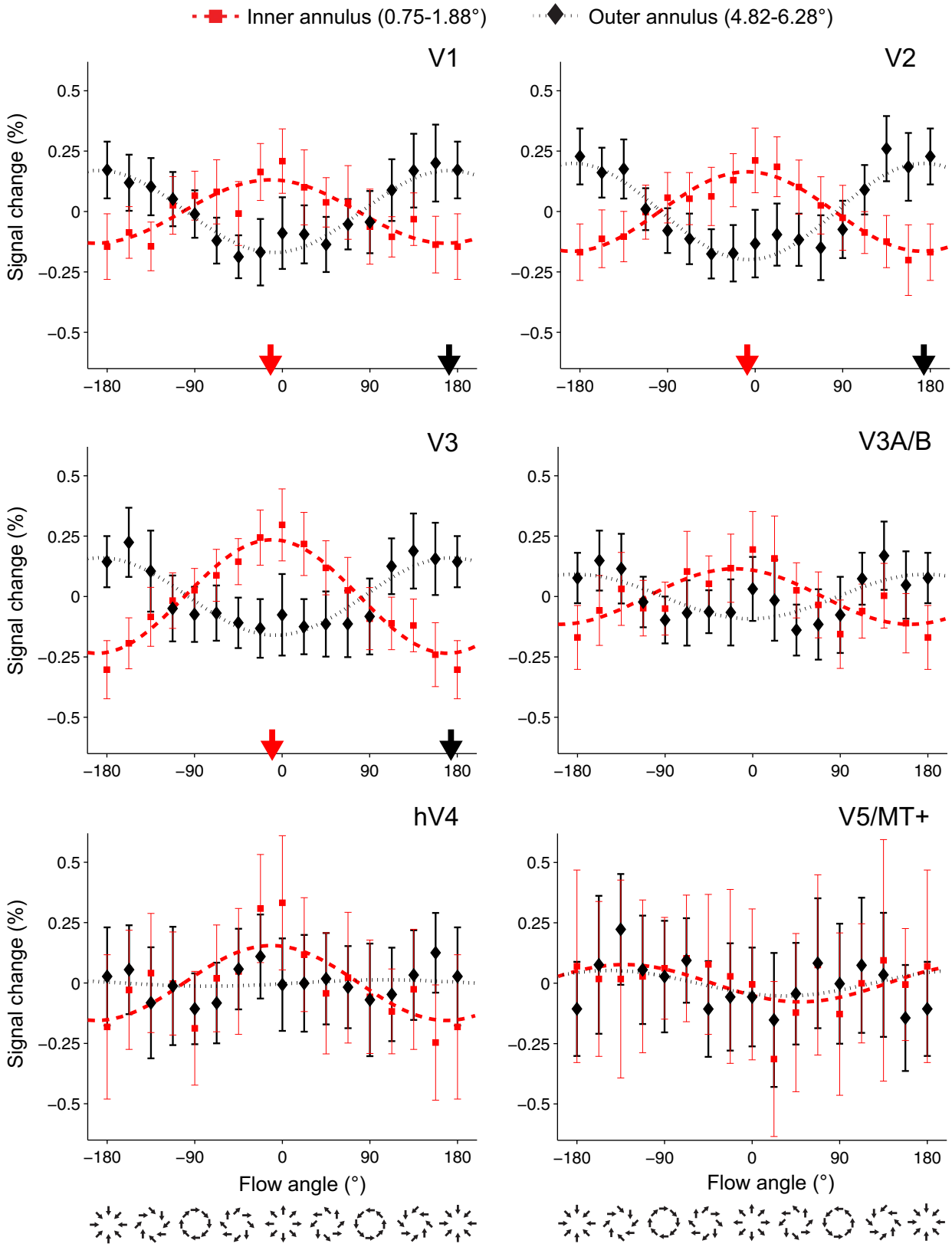

Fig. 5. Mean visual cortical responses in the wide-field stimulus configuration, with voxels masked by the SPM *t*-map of the GLM contrast of all motion flow angles vs. fixation ($p < 0.05$, uncorrected) in the narrow-annulus experiment. Each panel shows the mean BOLD percentage signal change (± 1 standard error) across the 4 subjects common to both experiments, at the 6 different visual regions of interest. Figure conventions are as in Fig. 3, where the symbols show the mean data at the positions of the 2 annuli, and smooth lines show the best-fitting cosinusoid, while the data for centripetal motion is wrapped so that it appears at both $\pm 180°$ on the abscissa. Red squares give the mean response where voxels were masked by the inner annulus *t*-map, and black diamonds where voxels were masked by the outer annulus *t*-map. Downward-pointing arrows on the abscissa show the phase of the best-fitting cosinusoid where the circular correlation was significant. The colour of the arrows is the same as the data symbols for the two annulus conditions.

Table 5
Results of circular correlations (r) and phase of the best-fitting cosinusoid for the wide-field stimulus experiment, masked by the SPM t-maps of significant activation (all cardinal flow angles vs. fixation) in the narrow annulus experiment.

	Annulus position			
	Inner (0.75–1.88°)		Outer (4.82–6.28°)	
ROI	r	Phase (°)	r	Phase (°)
V1	0.77*	−12	0.91**	171
V2	0.93**	−8	0.86***	173
V3	0.94**	−10	0.81***	174
V3A/B	0.62	−18	0.48	178
hV4	0.51	−11	0.02	105
V5/MT+	0.28	−131	0.14	−147

*$p < 0.05$; **$p < 0.01$; ***$p < 0.001$ (uncorrected), according to the null distribution of r values obtained via bootstrap procedure.

eccentricity range with the edge of the stimulus would be minimal, and yet there is still a clear change (at least in V2 and V3) in the shape of the anisotropies between the two innermost eccentricities and the 3rd eccentricity. Raemaekers et al. (2009) and Schellekens et al. (2013) report similar findings using a different stimulus and analysis to the present study. Further, by masking the ROIs by the SPM t-map from the narrow annulus experiment (see Fig. 5), the mean response in the wide-field stimulus experiment could be examined without referring at all to the eccentricity maps, yet the results in both cases (at the corresponding spatial locations) were very similar, suggesting that the shift in the anisotropies with eccentricity was not just a consequence of errors associated with the method of acquiring the eccentricity maps.

Ramachandran and Anstis (1990) reported that the perceived size of a stimulus aperture defined by kinetic signals alone can be influenced by the motion pattern presented therein. Centrifugal motion can cause an illusory increase in an aperture size while centripetal motion can cause it to appear to contract or shrink. It is possible that the shift in the direction of the radial biases with eccentricity (and as such, the edges of the stimulus aperture) as measured with the wide-field stimulus might be correlated with the opposing effects of perceived size with the radial motions of opposite direction. Activity in visual cortex is known to scale with illusions of perceived size (Fang et al., 2008; Murray et al., 2006; Sperandio et al., 2012). Sperandio et al. (2012) for instance found that the perceived (rather than the retinal) size of an afterimage was positively correlated with activity in human V1. It might be expected then that the illusory "looming" of a centrifugal stimulus would be correlated with a larger BOLD intensity at the aperture edge, and correspondingly, the apparent "shrinking" of a centripetal stimulus would be correlated with a decrease in BOLD intensity. Since the precise opposite of this was found it is unlikely that perceived size effects were a factor in the present set of experiments.

Altogether, the pattern of results across both the wide-field and narrow annulus experiments suggest important roles for V2 and V3 in the analysis of radial motion information. A preference for radial motion that shifts (toward centrifugal or centripetal) as a function of eccentricity has previously been described in areas V1–V3 (Raemaekers et al., 2009; Schellekens et al., 2013), although why this should be so remains something of a puzzle. Radial biases (for both motion direction and orientation) in mammals may have an anatomical basis in the retina, since retinal ganglion cell ontogenesis occurs in a radial pattern centred at the area centralis (Rapaport and Stone, 1984), which probably accounts for their radially-oriented receptive fields (Levick and Thibos, 1982) and dendritic fields (Leventhal and Schall, 1983). However, a retinal locus does not easily account for the opposite BOLD responses to centrifugal and centripetal motion in the wide-field stimulus, nor the functional shift in these anisotropies with eccentricity, and, furthermore, radial motion biases in human infants seem to emerge only after a significant period of postnatal development (Brosseau-Lachaine et al., 2008; Gilmore et al., 2007).

Prioritising the processing of certain complex motion flow patterns as a function of eccentricity may be a function of their well-known ecological relevance for the effective coordination of ego-motion through 3-D space (Gibson, 1950; Howard, 1982; Koenderink, 1986; Regan and Beverley, 1982). Complex motions provide important inputs for computations including the recovery of heading information (Crowell and Banks, 1993; Warren and Hannon, 1988), the estimation of time-to-contact of obstacles (Lee, 1980), and the control of postural sway (Holten et al., 2013; Lee and Aronson, 1974), among others (for reviews see Britten, 2008; Lappe et al., 1999). Centrifugal patterns might receive a weaker cortical representation at larger eccentricities because once the motion has passed a certain point in the periphery it becomes less likely that it indicates a risk of collision with the observer. In the same manner, centrifugal motion at the centre of gaze could indicate looming or approaching objects and potential hazards, and thereby receives an enhanced cortical representation (Regan and Beverley, 1978, 1979). A large centripetal flow pattern stimulating the periphery, may, in the opposite sense, be an important cue signalling the need for fast postural corrections in humans, as in the case of a backwards swaying observer (Edwards and Ibbotson, 2007), whereas centripetal motions at the centre of gaze are more likely to be associated with a receding object moving away from the observer. In the present study however, stimuli were not designed to simulate object motion and at no point did subjects report experiencing illusions of self-motion (linear vection).

As intimated in the Introduction, a potentially more mechanistic explanation for the dependence on eccentricity might lie in the spatiotemporal predictability of the pattern formed on the retina by the wide-field motion stimuli, not just as it relates to the movement of objects towards or away from the human head (as in optic flow). A number of recent studies have demonstrated the influence motion predictability, and stimulus predictability more generally, can have on visual perception and on activity in visual cortex. Roach et al. (2011) investigated the detection of visual targets consisting of low-contrast drifting sinusoidal luminance grating patches when they were briefly presented adjacent to a large high-contrast drifting sinusoidal inducer. When the target was in phase with the inducer, the target appeared as if it was a low-contrast continuation of the inducer. When targets were presented at the trailing edge of the inducer (such that the direction of the drifting motion pointed away from the target), detection thresholds were markedly higher than in the control case where no inducer was present. Detection was even more severely impaired when the target grating was presented at the leading edge of the inducer grating (such that the direction of the drifting motion pointed towards the target), but at the opposite phase. Roach et al. (2011) suggest that the visual system combines an internal forward prediction of the spatial pattern of the motion with the incoming sensory signal, and when the two are incongruent perception is degraded.

A number of recent fMRI (and MEG) studies have also indicated that stimulus inputs are integrated with internal assumptions of stimulus predictability to bias sensory representations, where generally there is a weaker cortical response to more predictable stimuli (Alink et al., 2010; den Ouden et al., 2010, 2012; Kok et al., 2012a, 2012b, 2013; Summerfield et al., 2008; Todorovic and de Lange, 2012; Todorovic et al., 2011). Alink et al. (2010) for instance showed that the BOLD response in V1 and V5/MT+ was reduced when stimulus direction or onset was predictable within the context of apparent motion; in other words the response in these areas increased as stimuli became less predictable. Prima facie, this result might seem to reflect the influence of attention: a less predictable and more surprising stimulus might trigger attentional enhancement of the cortical representation over a more predictable, less surprising one. However, an accompanying psychophysical experiment run by Alink et al. (2010) showed that subjects' detection rates for the predictable motion stimuli were actually greater than those for the unpredictable motion stimuli (see also Schwiedrzik et al., 2007), suggesting that there is a negative relationship between

the perceptual sensitivity to predictable motion stimuli as measured behaviourally and the amplitude of cortical activity in response to them.

The influence of motion predictability might explain the dependence on eccentricity for the motion anisotropies measured in the present study in the wide-field stimulus condition. Assuming that the global pattern formed by the complex motion across the visual field undergoes some form of spatiotemporal integration across motion detectors with appropriately aligned receptive fields (Burr et al., 1998; Morrone et al., 1995; Snowden, 1994), the path or trajectory that dots undergoing centrifugal motion trace across the retina could be considered more predictable at more eccentric positions closer to where the path terminates, and less predictable where the path begins, closer to the fovea. There is accordingly a weaker cortical response to the centrifugally moving pattern where it is more predictable (at larger eccentricities), and a greater response where it is least predictable (at smaller eccentricities). Of course, the situation is the complete opposite in the case of centripetal motion: there is more uncertainty associated with the motion trajectory where it first begins in the periphery, but it becomes more predictable as it approaches its focus point at the fovea (in the case of the stimuli used here). This idea is also supported by the differences between the wide-field stimulus condition and those presented within narrow annuli. Across the two stimulus configurations, the motion within the stimulated portions of the visual field did not change but the predictability of the moving spatial pattern did. With the narrow annuli the predictability was disrupted and consequently the interaction with eccentricity disappeared. The nature of the prediction is then more perhaps about a forward prediction of the moving spatial pattern, rather than a simple prediction of the motion direction itself (Roach et al., 2011).

Of course, care must be taken to consider the role of low-level visual interactions in conceptions of motion predictability. Neural activity is likely to be greater for appearing dot elements than persisting dot elements, something demonstrated previously with fMRI (Liu et al., 2006; Whitney et al., 2003). In the present stimulus, appearing elements were not predictable whereas those continuing along the motion trajectory (or disappearing at the trajectory's termination) were, so it is difficult to separate notions of "predictability" from a simple neural response to an onset transient occurring within a receptive field compared to a response to an offset transient. Other, non-direction selective populations are also more likely to respond strongly to an appearing element, although there is evidence that offset transients act as important timing references in visual processing (Bair et al., 2002; Clifford, 2002; Tadin et al., 2010). Dot density was maintained at a constant level across the spatial extent of all motion flow angle stimuli used here (according to the "wraparound" algorithm described in Clifford et al., 1999), meaning that the distribution of transients (whether onset or offset) was balanced across stimuli. However, the type of transient (onset or offset) varied depending on the flow angle of the stimulus – there would be mostly offset transients for a centripetal pattern and mostly onset transients for a centrifugal pattern. This was the first study to systematically map the response to wide-field complex motion patterns in human fMRI and this imbalance in the distribution of the type of visual transients was unavoidable in such patterns in order to keep dot density constant. It is probable that low-level factors also had an influence in previous fMRI studies of motion direction anisotropies that either simply used linearly translating dots (e.g. Giaschi et al., 2007; Raemaekers et al., 2009; Schellekens et al., 2013) or dealt with the issue of dot density and the distribution of transients in radial motion by setting the individual dot lifetime to be less than the total duration of the stimulus (e.g. Koyama et al., 2005; Morrone et al., 2000; Wall and Smith, 2008; Wall et al., 2008). One interesting direction for future research would be to explore the interaction between motion predictability and low-level responses to visual transients. By placing occluding annular surfaces over radial/complex motion stimuli it should be possible to disambiguate these influences: the reappearance of a moving element somewhere on the edge of the occluder could be made predictable or unpredictable on the basis of its trajectory before disappearing behind the occluder, though in both cases the low-level response to the onset transient at its reappearance would be the same.

The role of predictability in accounting for the present results fits within the context of a broader framework of predictive coding. Motion "predictability" might refer, as already discussed, to the ability to anticipate the trajectory of a transitory motion stimulus based on the spatial pattern it forms. Predictability might also be framed in a more probabilistic sense, based on the influence of prior expectations on perception, built upon the statistics of visual stimulation encountered during natural viewing. Broadly speaking, Bayesian predictive coding accounts have gained considerable popularity in recent years in explaining a number of aspects of perceptual and other brain functions (e.g. Clark, 2013; Dennett, 2013; de-Wit et al., 2010; Enns and Lleras, 2008; Friston, 2010; Summerfield and Egner, 2009). The basic premise of predictive coding models is that internally-generated, top-down priors are compared with sensory inputs. Activity in early sensory cortex represents the discrepancy, or residual error between the predicted and the sensory evidence, often as a result of feedback signals from higher areas where the comparison is made (Barlow, 1994; Friston, 2005, 2010; Lee and Mumford, 2003; Mumford, 1992; Rao and Ballard, 1999; Spratling, 2010; Yuille and Kersten, 2006). A lower cortical response to more predictable motion might therefore represent not a weaker representation but rather a sharpened or more efficient one, with a higher signal-to-noise ratio (Alink et al., 2010; de-Wit et al., 2010; Kok et al., 2012a; Murray et al., 2004).

Within a Bayesian predictive coding framework, Zhang et al. (2013) recently found that there is a strong perceptual prior for centrifugal motion in the visual periphery. This result is resonant with the more frequent occurrence of centrifugal motion in the periphery that accompanies the optic flow of a forward-moving observer (Bubka et al., 2008; Howard, 1982; Regan and Beverley, 1982; Zhang et al., 2013). It also agrees with the present findings and within the context of predictive coding accounts: if there is a strong prior for centrifugal motion in the periphery, then it makes sense that there should be a weaker cortical response to centrifugal motion at higher eccentricities, as found here and elsewhere (Raemaekers et al., 2009; Schellekens et al., 2013). The opposite may be true for centripetal motion. Understanding the role of stimulus predictability, and more generally, predictive coding, in neural mechanisms of motion perception (along with a careful consideration of low-level visual properties, such as responses to onset and offset transients) represents an interesting and important avenue for future investigation.

Acknowledgments

This work was supported by a National Health and Medical Research Council grant (C.W.G.C.; grant number APP1027258), an Australian Research Council (ARC) Future Fellowship (C.W.G.C.; grant number FT110100150), an ARC Post-doctoral Fellowship (T.L.W.; grant number DP11010217) and the ARC Centre of Excellence in Vision Science. The authors thank Dr Isabelle Mareschal, Dr Sam Solomon and Dr Damien Mannion for helpful discussions; Kirsten Moffatt and the MRI radiography team at St. Vincent's Hospital, Darlinghurst, and Marcus Johnson from SR Research for assistance in setting up the MR-compatible EyeLink system.

References

Albright, T.D., 1989. Centrifugal directional bias in the middle temporal visual area (MT) of the macaque. Vis. Neurosci. 2 (2), 177–188.

Alink, A., Schwiedrzik, C.M., Kohler, A., Singer, W., Muckli, L., 2010. Stimulus predictability reduces responses in primary visual cortex. J. Neurosci. 30 (8), 2960–2966. http://dx.doi.org/10.1523/JNEUROSCI.3730-10.2010.

Allman, J.M., Kaas, J.H., 1971. A representation of the visual field in the caudal third of the middle tempral gyrus of the owl monkey (*Aotus trivirgatus*). Brain Res. 31 (1), 85–105.

Amano, K., Wandell, B.A., Dumoulin, S.O., 2009. Visual field maps, population receptive field sizes, and visual field coverage in the human MT + complex. J. Neurophysiol. 102 (5), 2704–2718. http://dx.doi.org/10.1152/jn.00102.2009.
Apthorp, D., Cass, J., Alais, D., 2011. The spatial tuning of "motion streak" mechanisms revealed by masking and adaptation. J. Vis. 11 (7), 17. http://dx.doi.org/10.1167/11.7.17.
Bair, W., Cavanaugh, J.R., Smith, M.A., Movshon, J.A., 2002. The timing of response onset and offset in macaque visual neurons. J. Neurosci. 22 (8), 3189–3205 (doi: 20026257).
Ball, K., Sekuler, R., 1980. Human vision favors centrifugal motion. Perception 9 (3), 317–325.
Barlow, H.B., 1994. What is the computational goal of the neocortex? In: Koch, C., Davis, J. L. (Eds.), Large-scale neuronal theories of the brain. MIT Press, Cambridge, MA, pp. 1–22.
Bartels, A., Logothetis, N.K., Moutoussis, K., 2008. fMRI and its interpretations: an illustration on directional selectivity in area V5/MT. Trends Neurosci. 31 (9), 444–453. http://dx.doi.org/10.1016/j.tins.2008.06.004.
Beardsley, S.A., Vaina, L.M., 2005. Psychophysical evidence for a radial motion bias in complex motion discrimination. Vis. Res. 45 (12), 1569–1586. http://dx.doi.org/10.1016/j.visres.2004.11.025.
Beckett, A., Peirce, J.W., Sanchez-Panchuelo, R.M., Francis, S., Schluppeck, D., 2012. Contribution of large scale biases in decoding of direction-of-motion from high-resolution fMRI data in human early visual cortex. Neuroimage 63 (3), 1623–1632. http://dx.doi.org/10.1016/j.neuroimage.2012.07.066.
Brainard, D.H., 1997. The psychophysics toolbox. Spat. Vis. 10 (4), 433–436. http://dx.doi.org/10.1163/156856897X00357.
Britten, K.H., 2008. Mechanisms of self-motion perception. Annu. Rev. Neurosci. 31, 389–410. http://dx.doi.org/10.1146/annurev.neuro.29.051605.112953.
Brosseau-Lachaine, O., Casanova, C., Faubert, J., 2008. Infant sensitivity to radial optic flow fields during the first months of life. J Vis 8 (4), 1–14. http://dx.doi.org/10.1167/8.4.5.
Bubka, A., Bonato, F., Palmisano, S., 2008. Expanding and contracting optic-flow patterns and vection. Perception 37 (5), 704–711.
Burr, D.C., Morrone, M.C., Vaina, L.M., 1998. Large receptive fields for optic flow detection in humans. Vis. Res. 38 (12), 1731–1743.
Burr, D.C., Badcock, D.R., Ross, J., 2001. Cardinal axes for radial and circular motion, revealed by summation and by masking. Vis. Res. 41 (4), 473–481.
Clark, A., 2013. Whatever next? Predictive brains, situated agents, and the future of cognitive science. Behav. Brain Sci. 36 (3), 181–204. http://dx.doi.org/10.1017/S0140525X12000477.
Clifford, C.W.G., 2002. Response offset: the first sign of change? Trends Neurosci. 25 (7), 346.
Clifford, C.W., Beardsley, S.A., Vaina, L.M., 1999. The perception and discrimination of speed in complex motion. Vis. Res. 39 (13), 2213–2227.
Clifford, C.W., Mannion, D.J., McDonald, J.S., 2009. Radial biases in the processing of motion and motion-defined contours by human visual cortex. J. Neurophysiol. 102 (5), 2974–2981. http://dx.doi.org/10.1152/jn.00411.2009.
Cornelissen, F.W., Peters, E.M., Palmer, J., 2002. The Eyelink Toolbox: eye tracking with MATLAB and the Psychophysics Toolbox. Behav. Res. Methods Instrum. Comput. 34 (4), 613–617.
Crowell, J.A., Banks, M.S., 1993. Perceiving heading with different retinal regions and types of optic flow. Percept. Psychophys. 53 (3), 325–337.
Dakin, S.C., Mareschal, I., 2000. The role of relative motion computation in 'direction repulsion'. Vis. Res. 40 (7), 833–841.
den Ouden, H.E., Daunizeau, J., Roiser, J., Friston, K.J., Stephan, K.E., 2010. Striatal prediction error modulates cortical coupling. J. Neurosci. 30 (9), 3210–3219. http://dx.doi.org/10.1523/JNEUROSCI.4458-09.2010.
den Ouden, H.E., Kok, P., de Lange, F.P., 2012. How prediction errors shape perception, attention, and motivation. Front. Psychol. 3, 548. http://dx.doi.org/10.3389/fpsyg.2012.00548.
Dennett, D.C., 2013. Expecting ourselves to expect: the Bayesian brain as a projector. Behav. Brain Sci. 36 (3), 209–210. http://dx.doi.org/10.1017/S0140525X12002208.
de-Wit, L., Machilsen, B., Putzeys, T., 2010. Predictive coding and the neural response to predictable stimuli. J. Neurosci. 30 (26), 8702–8703. http://dx.doi.org/10.1523/JNEUROSCI.2248-10.2010.
Dubner, R., Zeki, S.M., 1971. Response properties and receptive fields of cells in an anatomically defined region of the superior temporal sulcus in the monkey. Brain Res. 35 (2), 528–532.
Duffy, C.J., Wurtz, R.H., 1991a. Sensitivity of MST neurons to optic flow stimuli. I. A continuum of response selectivity to large-field stimuli. J. Neurophysiol. 65 (6), 1329–1345.
Duffy, C.J., Wurtz, R.H., 1991b. Sensitivity of MST neurons to optic flow stimuli. II. Mechanisms of response selectivity revealed by small-field stimuli. J. Neurophysiol. 65 (6), 1346–1359.
Duffy, C.J., Wurtz, R.H., 1997. Medial superior temporal area neurons respond to speed patterns in optic flow. J. Neurosci. 17 (8), 2839–2851.
Dumoulin, S.O., Wandell, B.A., 2008. Population receptive field estimates in human visual cortex. Neuroimage 39 (2), 647–660. http://dx.doi.org/10.1016/j.neuroimage.2007.09.034.
Dumoulin, S.O., Bittar, R.G., Kabani, N.J., Baker Jr., C.L., Le Goualher, G., Pike, G.B., Evans, A.C., 2000. A new anatomical landmark for reliable identification of human area V5/MT: a quantitative analysis of sulcal patterning. Cereb. Cortex 10 (5), 454–463.
Edwards, M., Badcock, D.R., 1993. Asymmetries in the sensitivity to motion in depth: a centripetal bias. Perception 22 (9), 1013–1023.
Edwards, M., Ibbotson, M.R., 2007. Relative sensitivities to large-field optic-flow patterns varying in direction and speed. Perception 36 (1), 113–124.
Efron, B., Tibshirani, R.J., 1993. An introduction to the bootstrap. Chapman & Hall, New York.
Engel, S.A., 2012. The development and use of phase-encoded functional MRI designs. Neuroimage 62 (2), 1195–1200. http://dx.doi.org/10.1016/j.neuroimage.2011.09.059.
Engel, S.A., Rumelhart, D.E., Wandell, B.A., Lee, A.T., Glover, G.H., Chichilnisky, E.J., Shadlen, M.N., 1994. fMRI of human visual cortex. Nature 369 (6481), 525. http://dx.doi.org/10.1038/369525a0.
Engel, S.A., Glover, G.H., Wandell, B.A., 1997. Retinotopic organization in human visual cortex and the spatial precision of functional MRI. Cereb. Cortex 7 (2), 181–192.
Enns, J.T., Lleras, A., 2008. What's next? New evidence for prediction in human vision. Trends Cogn. Sci. 12 (9), 327–333. http://dx.doi.org/10.1016/j.tics.2008.06.001.
Fang, F., Boyaci, H., Kersten, D., Murray, S.O., 2008. Attention-dependent representation of a size illusion in human V1. Curr. Biol. 18 (21), 1707–1712. http://dx.doi.org/10.1016/j.cub.2008.09.025.
Fischer, E., Bülthoff, H.H., Logothetis, N.K., Bartels, A., 2012. Visual motion responses in the posterior cingulate sulcus: a comparison to V5/MT and MST. Cereb. Cortex 22 (4), 865–876. http://dx.doi.org/10.1093/cercor/bhr154.
Freeman, J., Brouwer, G.J., Heeger, D.J., Merriam, E.P., 2011. Orientation decoding depends on maps, not columns. J. Neurosci. 31 (13), 4792–4804. http://dx.doi.org/10.1523/JNEUROSCI.5160-10.2011.
Friston, K., 2005. A theory of cortical responses. Philos Trans R Soc Lond B Biol Sci 360 (1456), 815–836. http://dx.doi.org/10.1098/rstb.2005.1622.
Friston, K., 2010. The free-energy principle: a unified brain theory? Nat. Rev. Neurosci. 11 (2), 127–138. http://dx.doi.org/10.1038/nrn2787.
Friston, K.J., Ashburner, J.T., Kiebel, S.J., Nichols, T.E., Penny, W.D., 2007. Statistical parametric mapping: The analysis of functional brain images. Academic Press, London.
Furmanski, C.S., Engel, S.A., 2000. An oblique effect in human primary visual cortex. Nat. Neurosci. 3 (6), 535–536. http://dx.doi.org/10.1038/75702.
Geisler, W.S., 1999. Motion streaks provide a spatial code for motion direction. Nature 400 (6739), 65–69. http://dx.doi.org/10.1038/21886.
Giaschi, D., Zwicker, A., Young, S.A., Bjornson, B., 2007. The role of cortical area V5/MT + in speed-tuned directional anisotropies in global motion perception. Vis. Res. 47 (7), 887–898. http://dx.doi.org/10.1016/j.visres.2006.12.017.
Gibson, J.J., 1950. The perception of the visual world. Houghton Mifflin, Boston.
Gilmore, R.O., Hou, C., Pettet, M.W., Norcia, A.M., 2007. Development of cortical responses to optic flow. Vis. Neurosci. 24 (6), 845–856. http://dx.doi.org/10.1017/S0952523807070769.
Goddard, E., Mannion, D.J., McDonald, J.S., Solomon, S.G., Clifford, C.W., 2010. Combination of subcortical color channels in human visual cortex. J. Vis. 10 (5), 25.
Goddard, E., Mannion, D.J., McDonald, J.S., Solomon, S.G., Clifford, C.W., 2011. Color responsiveness argues against a dorsal component of human V4. J. Vis. 11 (4). http://dx.doi.org/10.1167/11.4.3.
Graziano, M.S., Andersen, R.A., Snowden, R.J., 1994. Tuning of MST neurons to spiral motions. J. Neurosci. 14 (1), 54–67.
Greenlee, M.W., 2000. Human cortical areas underlying the perception of optic flow: brain imaging studies. Int. Rev. Neurobiol. 44, 269–292.
Holliday, I.E., Meese, T.S., 2005. Neuromagnetic evoked responses to complex motions are greatest for expansion. Int. J. Psychophysiol. 55 (2), 145–157. http://dx.doi.org/10.1016/j.ijpsycho.2004.07.009.
Holliday, I.E., Meese, T.S., 2008. Optic flow in human vision: MEG reveals a foveo-fugal bias in V1, specialization for spiral space in hMSTs, and global motion sensitivity in the IPS. J Vis 8 (10), 1–24. http://dx.doi.org/10.1167/8.10.17.
Holten, V., Donker, S.F., Verstraten, F.A., van der Smagt, M.J., 2013. Decreasing perceived optic flow rigidity increases postural sway. Exp. Brain Res. 228 (1), 117–129. http://dx.doi.org/10.1007/s00221-013-3543-z.
Howard, I.P., 1982. Human visual orientation. John Wiley & Sons, Chichester, West Sussex.
Huk, A.C., Dougherty, R.F., Heeger, D.J., 2002. Retinotopy and functional subdivision of human areas MT and MST. J. Neurosci. 22 (16), 7195–7205.
Johnston, P.R., Rodriguez, J., Lane, K.J., Ousler, G., Abelson, M.B., 2013. The interblink interval in normal and dry eye subjects. Clin. Ophthalmol. 7, 253–259. http://dx.doi.org/10.2147/OPTH.S39104.
Koenderink, J.J., 1986. Optic flow. Vis. Res. 26 (1), 161–179.
Kok, P., Jehee, J.F., de Lange, F.P., 2012a. Less is more: expectation sharpens representations in the primary visual cortex. Neuron 75 (2), 265–270. http://dx.doi.org/10.1016/j.neuron.2012.04.034.
Kok, P., Rahnev, D., Jehee, J.F., Lau, H.C., de Lange, F.P., 2012b. Attention reverses the effect of prediction in silencing sensory signals. Cereb. Cortex 22 (9), 2197–2206. http://dx.doi.org/10.1093/cercor/bhr310.
Kok, P., Brouwer, G.J., van Gerven, M.A., de Lange, F.P., 2013. Prior expectations bias sensory representations in visual cortex. J. Neurosci. 33 (41), 16275–16284. http://dx.doi.org/10.1523/JNEUROSCI.0742-13.2013.
Kolster, H., Peeters, R., Orban, G.A., 2010. The retinotopic organization of the human middle temporal area MT/V5 and its cortical neighbors. J. Neurosci. 30 (29), 9801–9820. http://dx.doi.org/10.1523/JNEUROSCI.2069-10.2010.
Koyama, S., Sasaki, Y., Andersen, G.J., Tootell, R.B., Matsuura, M., Watanabe, T., 2005. Separate processing of different global-motion structures in visual cortex is revealed by fMRI. Curr. Biol. 15 (22), 2027–2032. http://dx.doi.org/10.1016/j.cub.2005.10.069.
Lagae, L., Maes, H., Raiguel, S., Xiao, D.K., Orban, G.A., 1994. Responses of macaque STS neurons to optic flow components: a comparison of areas MT and MST. J. Neurophysiol. 71 (5), 1597–1626.
Lappe, M., 2000. Computational mechanisms for optic flow analysis in primate cortex. Int. Rev. Neurobiol. 44, 235–268.
Lappe, M., Bremmer, F., van den Berg, A.V., 1999. Perception of self-motion from visual flow. Trends Cogn. Sci. 3 (9), 329–336.
Larsson, J., Heeger, D.J., 2006. Two retinotopic visual areas in human lateral occipital cortex. J. Neurosci. 26 (51), 13128–13142. http://dx.doi.org/10.1523/JNEUROSCI.1657-06.2006.

Larsson, J., Landy, M.S., Heeger, D.J., 2006. Orientation-selective adaptation to first- and second-order patterns in human visual cortex. J. Neurophysiol. 95 (2), 862–881. http://dx.doi.org/10.1152/jn.00668.2005.
Lee, D.N., 1980. The optic flow field: the foundation of vision. Philos. Trans. R. Soc. Lond. B Biol. Sci. 290 (1038), 169–179.
Lee, D.N., Aronson, E., 1974. Visual proprioceptive control of standing in human infants. Percept. Psychophys. 15, 529–532.
Lee, T.S., Mumford, D., 2003. Hierarchical Bayesian inference in the visual cortex. J. Opt. Soc. Am. A Opt. Image Sci. Vis. 20 (7), 1434–1448.
Leventhal, A.G., Schall, J.D., 1983. Structural basis of orientation sensitivity of cat retinal ganglion cells. J. Comp. Neurol. 220 (4), 465–475. http://dx.doi.org/10.1002/cne.902200408.
Levick, W.R., Thibos, L.N., 1982. Analysis of orientation bias in cat retina. J. Physiol. 329, 243–261.
Liu, J.V., Ashida, H., Smith, A.T., Wandell, B.A., 2006. Assessment of stimulus-induced changes in human V1 visual field maps. J. Neurophysiol. 96 (6), 3398–3408. http://dx.doi.org/10.1152/jn.00556.2006.
Ludbrook, J., 1998. Multiple comparison procedures updated. Clin. Exp. Pharmacol. Physiol. 25 (12), 1032–1037.
Maloney, R.T., Watson, T.L., Clifford, C.W.G., 2013. Human cortical and behavioral sensitivity to patterns of complex motion at eccentricity. J. Neurophysiol. 110, 2545–2556. http://dx.doi.org/10.1152/jn.00445.2013.
Mannion, D.J., Clifford, C.W.G., 2011. Cortical and behavioral sensitivity to eccentric polar form. J Vis 11 (6), 1–19. http://dx.doi.org/10.1167/11.6.17.
Mannion, D.J., McDonald, J.S., Clifford, C.W.G., 2010a. Orientation anisotropies in human visual cortex. J. Neurophysiol. 103 (6), 3465–3471. http://dx.doi.org/10.1152/jn.00190.2010.
Mannion, D.J., McDonald, J.S., Clifford, C.W.G., 2010b. The influence of global form on local orientation anisotropies in human visual cortex. Neuroimage 52 (2), 600–605. http://dx.doi.org/10.1016/j.neuroimage.2010.04.248.
Mardia, K.V., Jupp, P.E., 2000. Directional statistics. J. Wiley, Chichester.
Maunsell, J.H., Van Essen, D.C., 1983. Functional properties of neurons in middle temporal visual area of the macaque monkey. I. Selectivity for stimulus direction, speed, and orientation. J. Neurophysiol. 49 (5), 1127–1147.
McDonald, J.S., Mannion, D.J., Clifford, C.W., 2012. Gain control in the response of human visual cortex to plaids. J. Neurophysiol. 107 (9), 2570–2580. http://dx.doi.org/10.1152/jn.00616.2011.
Meese, T.S., Anderson, S.J., 2002. Spiral mechanisms are required to account for summation of complex motion components. Vis. Res. 42 (9), 1073–1080.
Morrone, M.C., Burr, D.C., Vaina, L.M., 1995. Two stages of visual processing for radial and circular motion. Nature 376 (6540), 507–509. http://dx.doi.org/10.1038/376507a0.
Morrone, M.C., Burr, D.C., Di Pietro, S., Stefanelli, M.A., 1999. Cardinal directions for visual optic flow. Curr. Biol. 9 (14), 763–766.
Morrone, M.C., Tosetti, M., Montanaro, D., Fiorentini, A., Cioni, G., Burr, D.C., 2000. A cortical area that responds specifically to optic flow, revealed by fMRI. Nat. Neurosci. 3 (12), 1322–1328. http://dx.doi.org/10.1038/81860.
Mumford, D., 1992. On the computational architecture of the neocortex. II. The role of cortico-cortical loops. Biol. Cybern. 66 (3), 241–251.
Murray, S.O., Schrater, P., Kersten, D., 2004. Perceptual grouping and the interactions between visual cortical areas. Neural Netw. 17 (5–6), 695–705. http://dx.doi.org/10.1016/j.neunet.2004.03.010.
Murray, S.O., Boyaci, H., Kersten, D., 2006. The representation of perceived angular size in human primary visual cortex. Nat. Neurosci. 9 (3), 429–434. http://dx.doi.org/10.1038/nn1641.
Orban, G.A., Lagae, L., Verri, A., Raiguel, S., Xiao, D., Maes, H., Torre, V., 1992. First-order analysis of optical flow in monkey brain. Proc. Natl. Acad. Sci. U. S. A. 89 (7), 2595–2599.
Pelli, D.G., 1997. The VideoToolbox software for visual psychophysics: transforming numbers into movies. Spat. Vis. 10 (4), 437–442. http://dx.doi.org/10.1163/156856897X00366.
Pigarev, I.N., Nothdurft, H.C., Kastner, S., 2002. Neurons with radial receptive fields in monkey area V4A: evidence of a subdivision of prelunate gyrus based on neuronal response properties. Exp. Brain Res. 145 (2), 199–206. http://dx.doi.org/10.1007/s00221-002-1112-y.
Pitzalis, S., Galletti, C., Huang, R.S., Patria, F., Committeri, G., Galati, G., Fattori, P., Sereno, M. I., 2006. Wide-field retinotopy defines human cortical visual area v6. J. Neurosci. 26 (30), 7962–7973. http://dx.doi.org/10.1523/JNEUROSCI.0178-06.2006.
Raemaekers, M., Lankheet, M.J., Moorman, S., Kourtzi, Z., van Wezel, R.J., 2009. Directional anisotropy of motion responses in retinotopic cortex. Hum. Brain Mapp. 30 (12), 3970–3980. http://dx.doi.org/10.1002/hbm.20822.
Raiguel, S., Van Hulle, M.M., Xiao, D.K., Marcar, V.L., Lagae, L., Orban, G.A., 1997. Size and shape of receptive fields in the medial superior temporal area (MST) of the macaque. Neuroreport 8 (12), 2803–2808.
Ramachandran, V.S., Anstis, S.M., 1990. Illusory displacement of equiluminous kinetic edges. Perception 19 (5), 611–616.
Rao, R.P., Ballard, D.H., 1999. Predictive coding in the visual cortex: a functional interpretation of some extra-classical receptive-field effects. Nat. Neurosci. 2 (1), 79–87. http://dx.doi.org/10.1038/4580.
Rapaport, D.H., Stone, J., 1984. The area centralis of the retina in the cat and other mammals: focal point for function and development of the visual system. Neuroscience 11 (2), 289–301.
Raymond, J.E., 1994. Directional anisotropy of motion sensitivity across the visual field. Vis. Res. 34 (8), 1029–1037.
Regan, D., Beverley, K.I., 1978. Looming detectors in the human visual pathway. Vis. Res. 18 (4), 415–421.
Regan, D., Beverley, K.I., 1979. Visually guided locomotion: psychophysical evidence for a neural mechanism sensitive to flow patterns. Science 205 (4403), 311–313.
Regan, D., Beverley, K.I., 1982. How do we avoid confounding the direction we are looking and the direction we are moving? Science 215 (4529), 194–196.
Roach, N.W., McGraw, P.V., Johnston, A., 2011. Visual motion induces a forward prediction of spatial pattern. Curr. Biol. 21 (9), 740–745. http://dx.doi.org/10.1016/j.cub.2011.03.031.
Sasaki, Y., Rajimehr, R., Kim, B.W., Ekstrom, L.B., Vanduffel, W., Tootell, R.B., 2006. The radial bias: a different slant on visual orientation sensitivity in human and nonhuman primates. Neuron 51 (5), 661–670. http://dx.doi.org/10.1016/j.neuron.2006.07.021.
Schellekens, W., Van Wezel, R.J., Petridou, N., Ramsey, N.F., Raemaekers, M., 2013. Integration of motion responses underlying directional motion anisotropy in human early visual cortical areas. PLoS One 8 (6), e67468. http://dx.doi.org/10.1371/journal.pone.0067468.
Schwiedrzik, C.M., Alink, A., Kohler, A., Singer, W., Muckli, L., 2007. A spatio-temporal interaction on the apparent motion trace. Vis. Res. 47 (28), 3424–3433. http://dx.doi.org/10.1016/j.visres.2007.10.004.
Seymour, K.J., Clifford, C.W., 2012. Decoding conjunctions of direction-of-motion and binocular disparity from human visual cortex. J. Neurophysiol. 107 (9), 2335–2341. http://dx.doi.org/10.1152/jn.01103.2011.
Smith, A.T., Wall, M.B., Williams, A.L., Singh, K.D., 2006. Sensitivity to optic flow in human cortical areas MT and MST. Eur. J. Neurosci. 23 (2), 561–569. http://dx.doi.org/10.1111/j.1460-9568.2005.04526.x.
Smith, A.T., Kosillo, P., Williams, A.L., 2011. The confounding effect of response amplitude on MVPA performance measures. Neuroimage 56 (2), 525–530. http://dx.doi.org/10.1016/j.neuroimage.2010.05.079.
Snowden, R.J., 1994. Motion processing in the primate cerebral cortex. In: Smith, A.T., Snowden, R.J. (Eds.), Visual detection of motion. Academic Press, London, pp. 51–83.
Sperandio, I., Chouinard, P.A., Goodale, M.A., 2012. Retinotopic activity in V1 reflects the perceived and not the retinal size of an afterimage. Nat. Neurosci. 15 (4), 540–542. http://dx.doi.org/10.1038/nn.3069.
Spratling, M.W., 2010. Predictive coding as a model of response properties in cortical area V1. J. Neurosci. 30 (9), 3531–3543. http://dx.doi.org/10.1523/JNEUROSCI.4911-09.2010.
Steinmetz, M.A., Motter, B.C., Duffy, C.J., Mountcastle, V.B., 1987. Functional properties of parietal visual neurons: radial organization of directionalities within the visual field. J. Neurosci. 7 (1), 177–191.
Summerfield, C., Egner, T., 2009. Expectation (and attention) in visual cognition. Trends Cogn. Sci. 13 (9), 403–409. http://dx.doi.org/10.1016/j.tics.2009.06.003.
Summerfield, C., Trittschuh, E.H., Monti, J.M., Mesulam, M.M., Egner, T., 2008. Neural repetition suppression reflects fulfilled perceptual expectations. Nat. Neurosci. 11 (9), 1004–1006. http://dx.doi.org/10.1038/nn.2163.
Swisher, J.D., Gatenby, J.C., Gore, J.C., Wolfe, B.A., Moon, C.H., Kim, S.G., Tong, F., 2010. Multiscale pattern analysis of orientation-selective activity in the primary visual cortex. J. Neurosci. 30 (1), 325–330. http://dx.doi.org/10.1523/JNEUROSCI.4811-09.2010.
Tadin, D., Lappin, J.S., Blake, R., Glasser, D.M., 2010. High temporal precision for perceiving event offsets. Vis. Res. 50 (19), 1966–1971. http://dx.doi.org/10.1016/j.visres.2010.07.005.
Tanaka, K., Saito, H., 1989. Analysis of motion of the visual field by direction, expansion/contraction, and rotation cells clustered in the dorsal part of the medial superior temporal area of the macaque monkey. J. Neurophysiol. 62 (3), 626–641.
Tanaka, K., Fukada, Y., Saito, H.A., 1989. Underlying mechanisms of the response specificity of expansion/contraction and rotation cells in the dorsal part of the medial superior temporal area of the macaque monkey. J. Neurophysiol. 62 (3), 642–656.
Todorovic, A., de Lange, F.P., 2012. Repetition suppression and expectation suppression are dissociable in time in early auditory evoked fields. J. Neurosci. 32 (39), 13389–13395. http://dx.doi.org/10.1523/JNEUROSCI.2227-12.2012.
Todorovic, A., van Ede, F., Maris, E., de Lange, F.P., 2011. Prior expectation mediates neural adaptation to repeated sounds in the auditory cortex: an MEG study. J. Neurosci. 31 (25), 9118–9123. http://dx.doi.org/10.1523/JNEUROSCI.1425-11.2011.
Tootell, R.B., Reppas, J.B., Kwong, K.K., Malach, R., Born, R.T., Brady, T.J., Rosen, B.R., Belliveau, J.W., 1995. Functional analysis of human MT and related visual cortical areas using magnetic resonance imaging. J. Neurosci. 15 (4), 3215–3230.
Vaina, L.M., 1998. Complex motion perception and its deficits. Curr. Opin. Neurobiol. 8 (4), 494–502.
Wall, M.B., Smith, A.T., 2008. The representation of egomotion in the human brain. Curr. Biol. 18 (3), 191–194. http://dx.doi.org/10.1016/j.cub.2007.12.053.
Wall, M.B., Lingnau, A., Ashida, H., Smith, A.T., 2008. Selective visual responses to expansion and rotation in the human MT complex revealed by functional magnetic resonance imaging adaptation. Eur. J. Neurosci. 27 (10), 2747–2757. http://dx.doi.org/10.1111/j.1460-9568.2008.06249.x.
Wandell, B.A., Winawer, J., 2011. Imaging retinotopic maps in the human brain. Vis. Res. 51 (7), 718–737. http://dx.doi.org/10.1016/j.visres.2010.08.004.
Wandell, B.A., Dumoulin, S.O., Brewer, A.A., 2007. Visual field maps in human cortex. Neuron 56 (2), 366–383. http://dx.doi.org/10.1016/j.neuron.2007.10.012.
Wang, H.X., Merriam, E.P., Freeman, J., Heeger, D.J., 2013. Motion direction preferences in human visual cortex. Program No. 120.13 Neuroscience 2013 abstracts. Society for Neuroscience, San Diego, CA (Online).
Warren, W.H., Hannon, D.J., 1988. Direction of self-motion is perceived from optical flow. Nature 336, 162–163. http://dx.doi.org/10.1038/336162a0.
Whitney, D., Bressler, D.W., 2007. Spatially asymmetric response to moving patterns in the visual cortex: re-examining the local sign hypothesis. Vis. Res. 47 (1), 50–59. http://dx.doi.org/10.1016/j.visres.2006.08.030.

Whitney, D., Goltz, H.C., Thomas, C.G., Gati, J.S., Menon, R.S., Goodale, M.A., 2003. Flexible retinotopy: motion-dependent position coding in the visual cortex. Science 302 (5646), 878–881. http://dx.doi.org/10.1126/science.1087839.

Xiao, Q., Barborica, A., Ferrera, V.P., 2006. Radial motion bias in macaque frontal eye field. Vis. Neurosci. 23 (1), 49–60. http://dx.doi.org/10.1017/S0952523806231055.

Yuille, A., Kersten, D., 2006. Vision as Bayesian inference: analysis by synthesis? Trends Cogn. Sci. 10 (7), 301–308. http://dx.doi.org/10.1016/j.tics.2006.05.002.

Zeki, S., Watson, J.D., Lueck, C.J., Friston, K.J., Kennard, C., Frackowiak, R.S., 1991. A direct demonstration of functional specialization in human visual cortex. J. Neurosci. 11 (3), 641–649.

Zhang, R., Kwon, O.S., Tadin, D., 2013. Illusory movement of stationary stimuli in the visual periphery: evidence for a strong centrifugal prior in motion processing. J. Neurosci. 33 (10), 4415–4423. http://dx.doi.org/10.1523/JNEUROSCI.4744-12.2013.

Zimmermann, J., Goebel, R., De Martino, F., van de Moortele, P.F., Feinberg, D., Adriany, G., Chaimow, D., Shmuel, A., Ugurbil, K., Yacoub, E., 2011. Mapping the organization of axis of motion selective features in human area MT using high-field fMRI. PLoS One 6 (12), e28716. http://dx.doi.org/10.1371/journal.pone.0028716.